Design of a Cubesat Based Radio Receiver to Detect the Global EoR Signature

by

Ashwini Jambagi

A Thesis Presented in Partial Fulfillment
of the Requirements for the Degree
Master of Science

Approved April 2019 by the
Graduate Supervisory Committee:

Philip Mauskopf, Co-Chair
James Aberle, Co-Chair
Georgios Trichopoulos

ARIZONA STATE UNIVERSITY

May 2019

ABSTRACT

The universe since its formation 13.7 billion years ago has undergone many changes. It began with expanding and cooling down to a temperature low enough for formation of atoms of neutral Hydrogen and Helium gas. Stronger gravitational pull in certain regions caused some regions to be denser and hotter than others. These regions kept getting denser and hotter until they had centers hot enough to burn the hydrogen and form the first stars, which ended the Dark Ages. These stars did not live long and underwent violent explosions. These explosions and the photons from the stars caused the hydrogen gas around them to ionize. This went on until all the hydrogen gas in the universe was ionized. This period is known as Epoch Of Reionization. Studying the Epoch Of Reionization will help understand the formation of these early stars, the timeline of the reionization and the formation of the stars and galaxies as we know them today. Studying the radiations from the 21cm line in neutral hydrogen, redshifted to below 200MHz can help determine details such as velocity, density and temperature of these early stars and the media around them.

The EDGES program is one of the many programs that aim to study the Epoch of Reionization. It is a ground-based project deployed in Murchison Radio-Astronomy Observatory in Western Australia. At ground level the Radio Frequency Interference from the ionosphere and various man-made transmitters in the same frequency range as the EDGES receiver make measurements, receiver design and extraction of useful data from received signals difficult. Putting the receiver in space can help majorly escape the RFI. The EDGES In Space is a proposed project that aims at designing a receiver similar to the EDGES receiver but for a cubesat.

This thesis aims at designing a prototype receiver that is similar in architecture to the EDGES low band receiver (50-100MHz) but is significantly smaller in size (small enough to fit on a PCB for a cubesat) while keeping in mind different considerations that affect circuit performance in space.

DEDICATION

To my parents

for without their constant support, encouragement and belief in me, Master's would have been just a dream

ACKNOWLEDGMENTS

I would like to thank Dr. Philip Mauskopf for giving an engineer like myself the opportunity to work in the Astronomy Instrumentation Lab and letting me experiment with more than one project in the lab. His guidance and approach towards the working of the projects have helped me learn a lot and grow technically and personally.

I would also like to thank my committee members Dr. James Aberle and Dr. Georgios Trichopoulos for guiding me throughout my graduate school. I am also grateful to Judd Bowman and Daniel Jacobs for giving me the opportunity to work on the EDGES In Space project and guiding me throughout the project.

I would like to extend my gratitude to Hamdi Mani, Eric Weeks, Leroy Johnson for helping me with the layout designs, assembly of the components and experimental setups for the testing of the receiver.

My sister Sneha Jambagi, my brother Mahendra Jambagi, my nephew Avyukt Chikaraddi and my brother-in-law Prasanna Chikaraddi deserve a special mention for their support and love made graduate school a possibility.

Lastly, I would like to thank my friends Namrata Gorantla, Deepika Eragamreddy, Reshma Naladala, Simarpreet Kaur, Nischal Naik, Jayanth Kumar, Ramkiran Krishnakumar and my aunt Kavita Tungal, my uncle Satya Hiredesai, my cousins Rhea and Harsha Hiredesai whose presence has made a foreign country feel like home.

TABLE OF CONTENTS

Page

CHAPTER Page

CHAPTER Page

LIST OF TABLES

Table Page

LIST OF FIGURES

Figure Page

Figure Page

CHAPTER 1

INTRODUCTION

1.1 Timeline of the Universe

The universe is estimated to have formed 13.7 billion years ago [1]. Since then it has undergone many changes which astronomers and cosmologists have tried to study and explain. Over the past century many studies and experiments have been conducted and the knowledge of the formation of the universe as we know it today has greatly increased. The Big Bang cosmological model is accepted across the community and describes the formation and evolution of the universe to the present day.

13.7 billion years ago the universe was very hot and very dense. This hot and dense phase is also known as the Big Bang. The universe was hot and dense enough that subatomic particles were being created and destroyed all the time. The universe constituted of particles which were in the form of radiation such as photons. These particles were ionized due to which the universe was opaque. Light did not travel very far before being absorbed or redirected due to the ionized particles [2].

From its formation the universe began rapidly expanding and cooling. Until 10^{-35} seconds after the Big Bang the universe went under a very rapid expansion by a factor of around 10^{60}. This phase is known as the cosmic inflation [3]. After about three minutes from the Big Bang, the matter that made up the universe was fixed – about three portions of Hydrogen and one portion of Helium [4]. The universe was to remain this way for the next few hundred thousand years.

After around 400,000 years after the Big Bang the universe had cooled down to 3000 Kelvin. This was cool enough for the formation of atoms by combining electrons

and protons. This formation of atoms led to the universe becoming transparent and allowing light to travel further in space. We see this light today as Cosmic Microwave Background (CMB). The expansion of the universe has led to the increase in the wavelength of the CMB and the CMB can be seen today in the microwave wavelengths [5]. This increase in the wavelength of the radiation over time results in redshift. From 400,000 years to the 400 million years after the Big Bang are known as the Dark Ages. During this period the universe consisted of neutral hydrogen and helium gas. Some of the regions of the universe were denser than others and had more gravitational pull. This gravitational pull caused the regions to get denser and hotter. This process would go on for until these dense regions were hot enough to form stars [6].

After the dark ages the universe has cooled down to a few hundred degrees. The regions that had kept getting denser and hotter now had centers hot enough to burn the hydrogen and form the first stars. These stars did not live very long and were made mostly of hydrogen and helium and some of it was fused into heavier elements. These stars underwent some violent explosions and created heavier elements. These explosions ionized the neutral hydrogen in the universe. The ionization went on for a few million years until the universe was completely ionized. This period is known as Epoch of Reionization [7].

As more stars were formed, the stars grouped together to form galaxies. These galaxies collided and merged to form larger galaxies. During this time the universe continued to expand. This expansion led to galaxies moving further apart from each other causing fewer collisions. The collisions of the galaxies caused gas and dust to be thrown around. Around 9 billion years after the Big Bang the Sun was formed from one such cloud of gas and dust. The gas and dust leftover from the cloud after the formation of the sun led to the formation of the solar system over a few hundred million years [8].

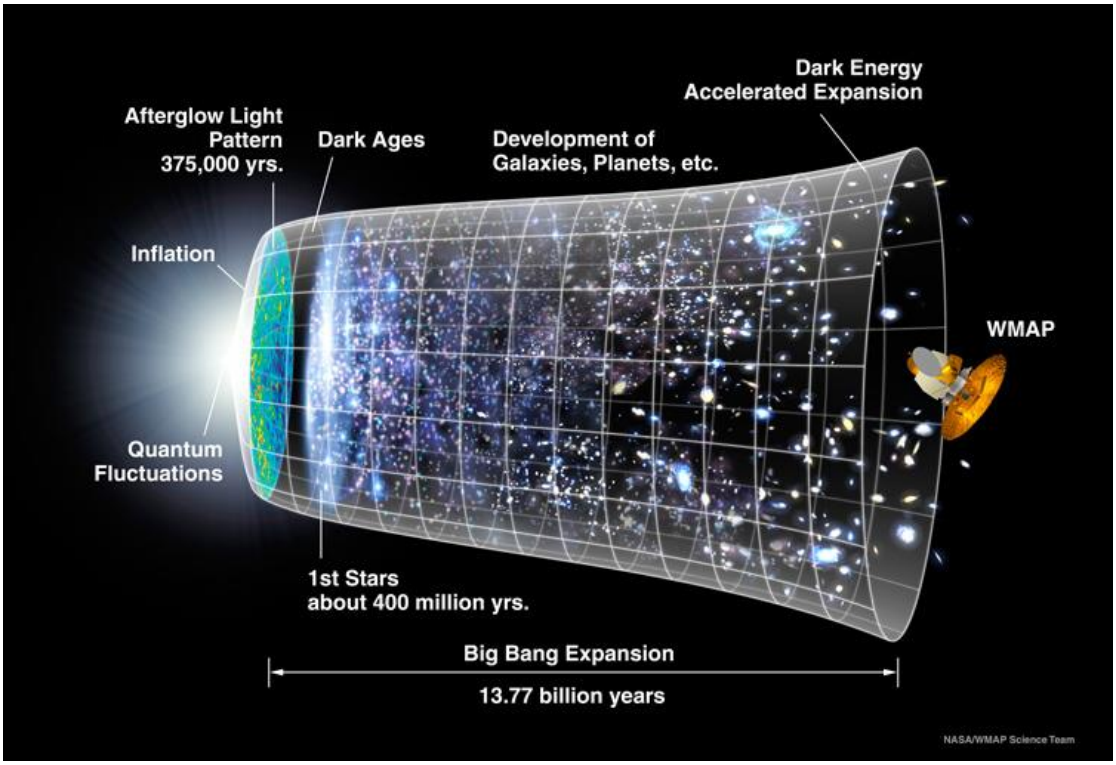

Figure 1.1 Timeline of the Universe [9]

1.2 Why Study the Epoch of Reionization (EoR)?

The Epoch of Reionization is the time during which the gas in the universe, mainly hydrogen went from being completely neutral to being completely ionized by the first sources of light. The first stars were formed due to the stronger gravitational pull from the denser objects in the universe which collapsed due to their own gravitational pull. These stars emitted radiation which ionized the neutral gas in the universe. The formation of the stars was the end of the Dark Ages. Very little is known about when these stars were formed and when the reionization started to occur. Understanding the formation of these early stars will help us understand the formation of the stars and the galaxies as we know today. These early stars greatly influenced the formation of the structures of the universe and the evolution of the universe.

At the beginning the first stars ionized the neutral gas around them and bubbles of ionized gas were formed around these stars. As more and more bubbles were formed, they started to overlap and more and more of the neutral universe was exposed to energy that ionized it. The ionization was faster towards the end. As more of the universe was ionized more light could escape and travel further. We study the universe by studying this light using various methods to detect it.

The 21cm line in neutral hydrogen, redshifted to below 200MHz is a potential means of studying the early phase of reionization. Splitting of the hydrogen due to the interaction between the protons and electrons spins leads to the 21cm line. The rest-frame frequency of the 21cm line is 1.4GHz [10]. The interaction between the magnetic moment of the proton and the magnetic moment of the electron is known as spin-spin coupling. Transition of the hydrogen atom from the ground state to the ionized state leads to the release of a photon which has as wavelength of 21cm [11]. Rest-frame frequency is the frequency of the light from the source if it were measured by an observing object adjacent to the source under the conditions that the observing object is moving with the same speed as the source in the same direction [12]. Studying the radiations in 21cm line can give us details such as density, temperature and velocity of the isolated early stars and the neutral media around them. This information could help us deduce the early history of structure formation. So far, the EDGES result from 2018 is the only detection of neutral hydrogen from this time of the universe formation [13].

1.3 Projects to Study EoR

Various ongoing experiments are being conducted to detect the global redshifted 21 cm EoR signature. The experiments can be broadly divided into two

categories based on the approach used to probe the EoR signature. The first approach uses interferometric arrays. These experiments provide us with a lot more information as we can control the measurements better and calibrate more accurately. But these experiments are more expensive to build and maintain [14]. Some examples of such experiments are **Lo**w **F**requency **AR**ray (LOFAR), **M**urchison **W**idefield **A**rray (MWA), **P**recision **A**rray to **P**robe **E**poch of **R**eionization (PAPER), **H**ydrogen **E**poch of **R**eionization **A**rray (HERA), **G**iant **M**etrewave **R**adio **T**elescope (GMRT) and **21 C**entimeter **A**rray (21CMA) [15].

The second approach measures the global radio signal averaged over the entire sky averaged as a function of frequency. Such experiments are relatively cheaper to build and maintain. But deciphering useful information from the received signal can be a challenge due to the radio frequency interference (RFI) and noise. Calibration of such devices is also harder and requires more accuracy to extract the data from the received signal [14]. This approach is being used by EDGES and will be continued to use in EDGES in Space. Details of EDGES and some other experiments using this approach are discussed in the following sections.

1.3.1 **E**xperiment to **D**etect the **G**lobal **E**oR **S**ignature (EDGES)

EDGES is a collaboration between ASU and MIT. The funding is from U.S. National Science Foundation (NSF) and site support from Australian Commonwealth Scientific and Industrial Organization (CSIRO) [16]. EDGES is deployed in the Murchison Radio-astronomy Observatory (MRO) in Western Australia due to its radio quiet conditions as low as -240dBWm^{-2}Hz^{-1} below 200MHz [17].

1.3.1.1 Instrument

The experiment consists of two instruments: the high band instrument and the low band instrument. The high band instrument operates in the frequency range of 100-200MHz while the low band instrument operates from 50-100MHz. The high band and the low band instruments have identical architectures designed for their respective frequency ranges. The antennas are scaled copies of each other [16].

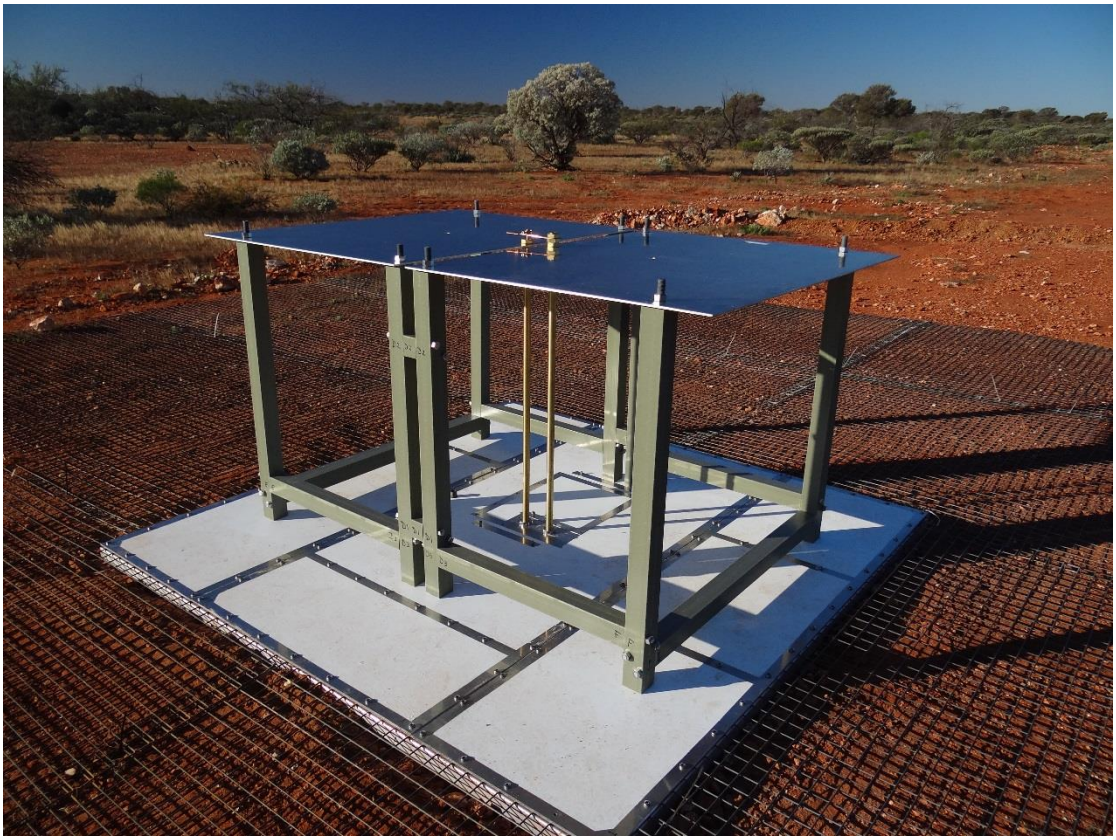

Figure 1.2 Low band Antenna [16]

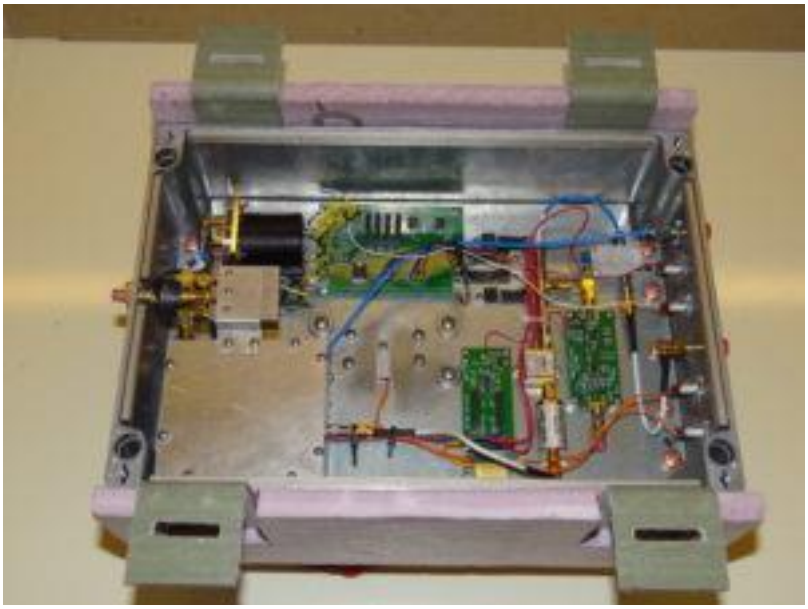

Figure 1.3 EDGES Receiver [16]

Figure 1.4 EDGES Experiment at MRO [16]

The first component in the instruments is the antenna which is a blade dipole antenna, which replaced the four-point antenna as it provides lower beam chromaticity which is contamination of the signal due to reflections. The ground plane of the antenna is a 5mx5m metal mesh (10mx10m for the low-band instrument) placed on the ground. It is followed by receiver directly below the antenna ground plane. The antenna and the receiver are connected via a Roberts balun [18]. The receiver below the antenna constitutes the front-end electronics. The receiver has switching capability to provide for the remote measurement of the antenna reflection coefficient and a remote calibration unit for the Vector Network Analyzer (VNA). The switching stage is followed by the first stage of low noise amplification, second stage of amplification and filtering in that order. The receiver also contains noise references. All of these components are placed in a metal enclosure. The receiver temperature is maintained at 25^{o}C at all times and temperature stability of better than 0.1^{o}C is achieved using thermal controller and a thermistor installed inside the receiver. The receiver output is fed to the back-end electronics via a 100m long coaxial cable where it is further amplified and filtered. This signal is then fed to an ADC. The ADC and the back-end electronics are placed in an EMI-shielded equipment rack [19].

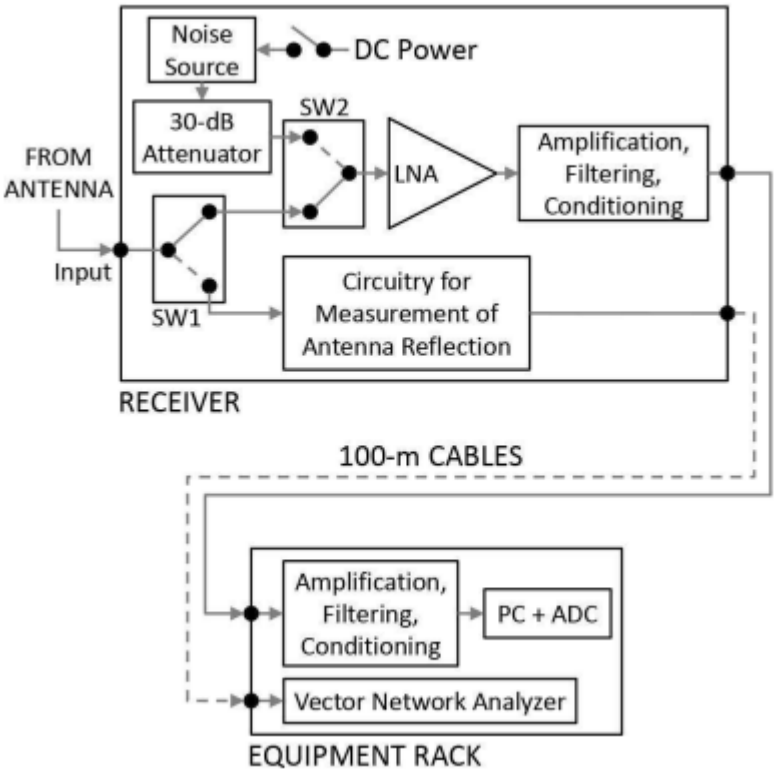

Figure 1.5 Block Diagram of EDGES Instrument [18]

1.3.1.2 Calibration

The signal obtained at the output of the instrument through the ADC consists of many uncertainties and errors due to the mismatch between the antenna and the receiver input. These unknown error quantities can get amplified in the receiver chain and also get reflected back into the antenna and transmitted by the antenna which can result in wrong measurement of the antenna temperature [20]. To account for these errors the EGDES instrument uses a unique calibration procedure. The receiver is calibrated in the lab before being deployed on site and mechanism for remote calibration is also incorporated in the receiver design. The measurements made in the lab during the calibration and the calibration measurements in the field are used to correct for the

errors and uncertainties and extract accurate and useful information from the signal measured by the instrument.

In the lab the receiver is calibrated at 25^{o}C for one day, at 35^{o}C for 3 days, at 15^{o}C for two days and finally at 25^{o}C again for another day. During these calibration times the Low Noise Amplifier (LNA) switches between three loads ambient load, hot load and antenna simulator. Along with this the receiver is calibrated for three standards loads of open, short and matched load using the SP4T switch which is present in the Circuitry for measurement of Antenna Reflection block in Figure 1.5. The SP4T is then set to connect to the receiver input and measurements are made for ambient load, antenna simulator, long cable with open termination and long cable with short termination. The spectra from these measurements are recorded and used for error correction [21]. In the field the LNA switches between the antenna, load and load plus noise source and measures each of them for 13 seconds. These measurements are used to determine the final calibrated antenna temperature [19].

1.3.1.3 Results

Over the years EDGES has collected a lot of data and great amount of analysis has been done on this data to obtain useful information about Epoch of Reionization. Using the data from the high band instrument EDGES has been able to rule out various tanh-based models for reionization and various Gaussian models for 21cm absorption trough that have been proposed so far [22]. With the help of the spectra recorded from the EDGES low band instrument has been able to detect an absorption profile between 50MHz and 100MHz centered around 78MHz [23].

1.3.2 **S**onda **C**osmológica de las **I**slas Para la **D**etección de **Hi**drógeno Neutro (SCI-HI) and **P**robing **R**adio **I**ntensity at High-**Z** from **M**arion (PRIZM)

The SCI-HI experiment measures the 21cm EoR signature using a single antenna and a sampling system and is deployed at Isla Guadalupe, a Mexican biosphere reserve located in the Pacific Ocean. The antenna is a four-square antenna operating form 40-130 MHz with over 90% antenna coupling efficiency from 55-90MHz. The sampling system consists of multiple stages of amplification and filtering to remove the RFI and aliasing signals. A switching stage exists between the sampling stage and antenna to measure spectra from known terminations namely 50Ω, 100Ω and short. The sampling stage also consists of GE PCIe digitizer board and a PC [24].

PRIZM is the second-generation setup of SCI-HI deployed on Marion island in the sub-Antarctic. The experiment consists of two dual-polarization radiometers with center frequencies of 70MHz and 100MHz. The antennas used are four-squared HIBiscus antenna design [25]. The antennas provide optimized performance over frequency range of 50-90MHz for the 70MHz centered radiometer and 70-130MHz for the 100MHz centered radiometer. The antennas are immediately followed by the first-stage electronics placed below the antenna petals. This stage of electronics consists of the switching system to switch between the calibration standards of the 50Ω, 100Ω and short and the first low noise amplification stage. The second-stage of electronics is connected to the first stage using 50m long coaxial cable. This is done to separate the two antennas and avoid interference of the signals from the antennas with each other. The second-stage electronics is enclosed on a Faraday cage and consists of second stage of amplification followed by a filtering stage. The output of this stage is fed to a readout circuit which is a Smart Network ADC Processor. The data is then given to Raspberry

Pi computers. The power to the entire experiment is provided using 8 12V, 170Ah Lead Crystal batteries [25].

1.3.3 **S**haped **A**ntenna Measurement of Background **RA**dio **S**pectrum 2 (SARAS 2)

SARAS 2 is a radiometer that operates in the frequency range of 40-200 MHz deployed at the Timbaktu Collective in Southern India. The radiometer consists of four sub-systems – the antenna, the receiver, a signal processing unit and a digital spectrometer. The antenna is a spherical monopole antenna placed above a disc. The receiver is placed right below the antenna and it amplifies the signal from the antenna, the reference and the calibration noise source. It generates a linear combination of these signals and transmit them through optical fibers. The signal processing unit converts the signals from optical to radio frequency and performs filtering of the signals. This signal is then sent to the digital spectrometer that produces the sky spectra [26].

1.3.4 **L**arge aperture **E**xperiment to Detect the **D**ark **A**ges (LEDA)

LEDA is a multi-antenna experiment that is part of the Long Wavelength Array installed at the Owens Valley Radio Observatory. LEDA consists of 5x2 complete radiometers. Each radiometer composes of four main components namely antenna, front-end receiver, back-end analog systems and digital systems. The antenna is directly connected to the front-end electronics (FE). The FE converts the balanced antenna to unbalanced 50Ω using a balun and amplifies and filters the signal and sends it to the back-end electronics via a buried co-axial cable. The back-end analog system further amplifies and filters the signal and prepares it to be digitized. The signals are sent to the digitizer using Category-7A Ethernet cables [27].

1.3.5 **B**roadband **I**nstrument for **G**lobal **H**ydr**O**gen **R**eio**N**isation **S**ignal (BIGHORNS)

The BIGHORNS experiment is a total power radiometer deployed in the remote radio quiet region of Western Australia. The first component in the chain is a biconical antenna followed by analog electronics made of off-the-shelf components. The analog chain consists of the first low noise amplifier and a switching mechanism to switch between the antenna and reference source which is a 50Ω termination. It is powered by a bias tee. The signal then travels to the next component of the RF-shielded rack via a 100m cable. The rack provides the second stage of amplification and then filters the signal. This signal is then provided to a Bedlam board (a High-Speed Digital Signal Processing board) which has built-in analog-to-digital converters and FGPAs. These FPGAs are configured as spectrometers. The digital signals from the BEDLAM board are transmitted over ethernet cables to a PC [28].

1.4 Why Put EDGES in Space?

The Ionosphere is the ionized part of the Earth's atmosphere. i.e. it consists of free electrons and positively charged atoms and molecules. This ionization is mainly due to the ultraviolet radiation from the sun. The layer extends from about 37 miles to 620 miles above the earth's surface. The ionosphere can be primarily divided into three layers namely D, E and F. The layer D is the one closest to the earth and is approximated to go from 37 miles to 56 miles from the earth's surface. E is the middle layer and goes approximately from 56 miles to 93 miles from the earth's surface. The F layer goes from 93 miles to 310 miles from the earth's surface. This is the layer with the highest electron density. At night time the level of ionization in layers D and E reduces significantly [29].

Due to the ions present in the ionosphere the radio waves travelling through it undergo refraction, absorption and thermal emission. These effects cause the radio waves to undergo different changes at different frequencies. The refraction of the radio waves occurs due to the changing density of the ionosphere, the majority of which is due to the F layer. This refraction causes a ground-based radio antenna to record signal from a larger region of sky resulting in excess antenna temperature [30]. The attenuation of the radio waves due to absorption occurs mainly in the D layer [30]. The effect of refraction and the absorption on the radio waves is inversely proportional to the square of frequency [30]. Hence these effects are seen significantly in our signal of interest.

Another component adding to the difficulty of measurements of the global 21 cm signal is the RFI due to man-made components such as transmitters for long distance communication at these frequencies. The levels at about 45MHz are about -175dBWm^{-2}Hz^{-1} and about -100dBWm^{-2}Hz^{-1} below 20MHz [31]. These signals can manifest as intermodulation products in the receiver and cause linearity issues making the receiver design complex and challenging.

One way to overcome the challenges arising from the man-made and ionosphere RFI is to put the receiver in space. The receiver can be put in space in Low Earth Orbit (LEO), but the effective antenna temperature would exceed 10^9K due to the signals from a single FM transmitter in the line of sight of the receiver as opposed to the required 1mK. In Geosynchronous Earth Orbit (GEO) the antenna temperature would be around 10^8K [32]. Due to these reasons the far side of the moon presents a much better environment for the receiver as the moon has almost negligible ionosphere and the far side is shielded from the RFI from the earth [33]. The EDGES in Space receiver is proposed to be deployed on the far side of the moon due to these reasons.

1.5 Other Projects Similar to EDGES in Space

1.5.1 **D**ark **A**ges **R**adio **E**xplorer (DARE)

DARE is a collaboration between University of Colorado, Boulder and National Aeronautics and Space Administration (NASA). It will be a lunar orbiter mission designed to operate from 40-120MHz. The instruments are being developed at Jet Propulsion Laboratory (JPL). The antenna for this project will be a bi-conical dipole. The spacecraft will have two dipoles orthogonal to each other to provide for different polarizations. The antennas are followed by a receiver which amplifies the signal before it is sent to the digital spectrometer. The receiver has an LNA as its first stage followed by a switching stage to provide for load switching. The reference load is a resistor. The amplifiers after the antenna and after the resistor are matched pairs providing similar performance. The signals coming from the different antennas are provided to different LNAs. To combine these signals a 180^{o} hybrid coupler is used after the switching stage. The receiver is powered by 12V DC from electronics assembly. A digital polyphase spectrometer implemented by space-qualified FPGA follows the receiver and an ADC [34].

1.5.2 **N**etherlands **C**hina **L**ow-Frequency **E**xplorer (NCLE)

Chang'e 4 is a lunar lander and rover deployed on the south pole region of the far side of the moon. It is a backup to the Chang'e 3 mission. Landing and roving on the far side of the moon requires a relay satellite. The NCLE is a low-frequency scientific receiver mounted on this relay satellite for Chang'e 4 Queqiao. The Queqiao was launched in May 2018 [35]. The receiver project is a collaboration between ASTRON, Radboud University, Innovative Solutions in Space (ISIS) and National Astronomical Observatory of China (NAOC). The NCLE contains three co-located 5

m monopole antennas. The signals received by the antenna are digitized in a DSP system. The digital information undergoes implementation of dedicated scientific and mathematical functions such as Fourier Transform. This implementation is done in a software defined radio system [36].

1.6 Thesis Focus

The current front-end electronics of the EDGES receiver is big enough to require a metal enclosure bigger in size than a shoe box. To put EDGES in space we would need a receiver that is physically smaller. This thesis discusses the design and build procedure of the RF chain of the EDGES receiver physically small enough to be put in a cubesat.

The receiver will be designed to replicate only the low-band instrument of the EDGES receiver and will be designed for the frequency range of 10-110MHz with the best performance for the frequency range of 50-100MHz. The reason to extend the lower frequency range to 10MHz is to be able to reuse the same receiver for low frequency cosmology below 30MHz to study the Cosmic Dawn. The temperature control mechanism currently being implemented in the EDGES receiver will not be continued in this first version of the EDGES In Space receiver. Provision will be made to be able to implement the (Vector Network Analyzer) VNA in the future but will not be done in this version of the design. The current receiver architecture will be maintained in the new receiver to make it possible to run the current software scripts with making as minimal amount of changes as possible. The SP4T switch position will be interchanged with the SPDT switch right after the antenna. This will be done to make remote measurement reflection coefficient of the LNA along with that of the antenna.

The SP4T switch will be replaced by a SP6T switch to add more calibration standards making the measurements more accurate.

The upcoming chapters will discuss in more detail the simulations, board design procedure and the result obtained from the receiver.

CHAPTER 2

DESIGN AND SIMULATION

The procedure adopted for the design of the receiver can be broadly divided into three steps. The first step was to finalize each component that will be used to build the receiver. The second step was to simulate the performance of these components after they are connected appropriately. This was done by simulating the S-Parameters in Advanced Design System (ADS) software by Keysight. The third step was to design the layout of the PCB to make the connections between each of the components and make connections for power supply and digital logic. The details of these steps have been described in the following sections.

2.1 Switch

The EDGES receiver consists of two SPDT switches and a SP4T switch. The SP4T switch is a component of the 'Circuitry for Measurement of Antenna Reflection' block of Figure 1.5. Moving forward the switching mechanism will be slightly altered. The SP4T switch will be replaced with a SP6T switch making it possible to add two more calibration standards and improving the accuracy of the antenna reflection measurement. The position of the SP6T switch will be right after the antenna. This will ensure that the calibration standards and the antenna measurements will be done at the same reference point. Changing the switch position will require a minor change in the code that is being used to calibrate the receiver. The insertion loss of this switch will add to the noise figure of the receiver as it will be in the path between the antenna and the amplifier.

The SPDT and the SP4T switches are mechanical switches. These switches have the advantage of low insertion loss which help keep the overall noise figure of the receiver low. But these switches have a limited life time (~10 million cycles) [37] and the performance degrades with time. In our application we will not be able to replace components once the cubesat is deployed. We would want a component to retain its performance capabilities throughout the project lifetime. These switches also require higher power to operate, something that won't be adequately available in space. Other disadvantages of mechanical switches would be slow switching times and bigger physical size. Microelectromechanical (MEMS) switches provide low insertion loss and faster switching time with lesser power consumption and are small in size. They have more lifetime than those of mechanical switches (billion cycles) [38] but we want a component whose performance is not limited by time. Which is why for this design electrical switches will be used. They operate at lower power, provide faster switching, are physically small and can ideally be used for infinite amount of time period, but they will have higher insertion loss.

The switches used for this design are Mini-circuits JSW6-33DR+ for the SP6T and JSW2-63VHDRG+ for the SPDTs. The performance of these switches simulated using the S-parameters provided by the manufacturer are plotted below. The plots are shown for RF1 port of the switch ON for both the switches. The isolation is between RF1 and RF2 when RF1 is ON for both switches.

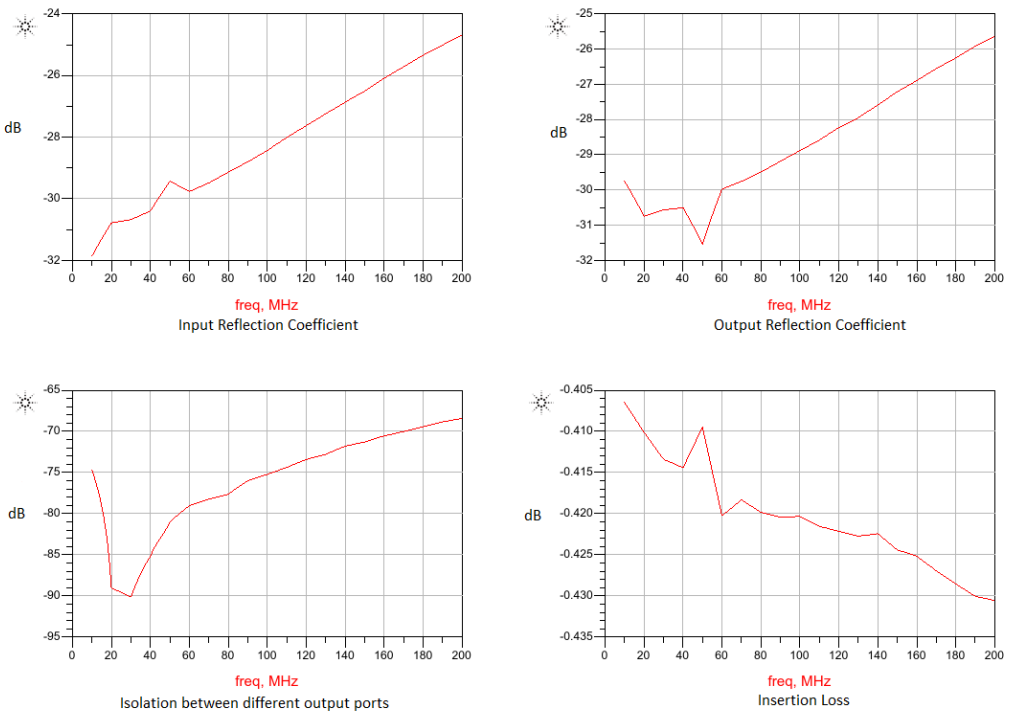

Figure 2.1 Performance of the SP6T Switch

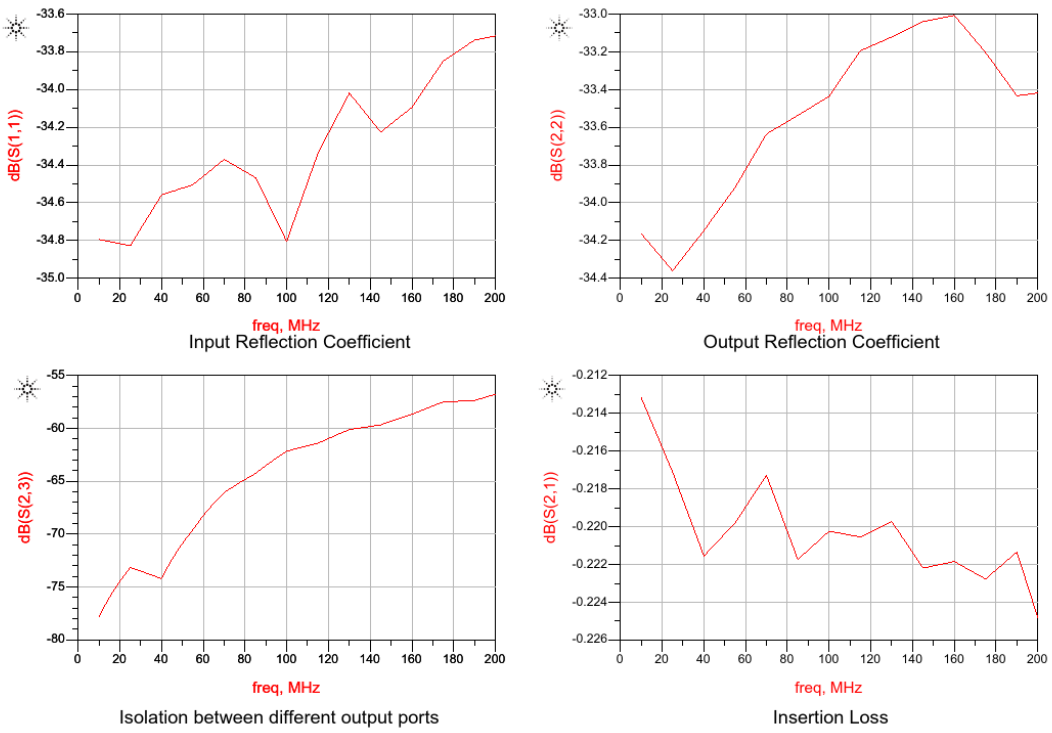

Figure 2.2 Performance of the SPDT Switch

The JSW6-33DR+ performance was measured in the lab using the evaluation board TB-724+ provided by Mini-circuits and the parameters are plotted below.

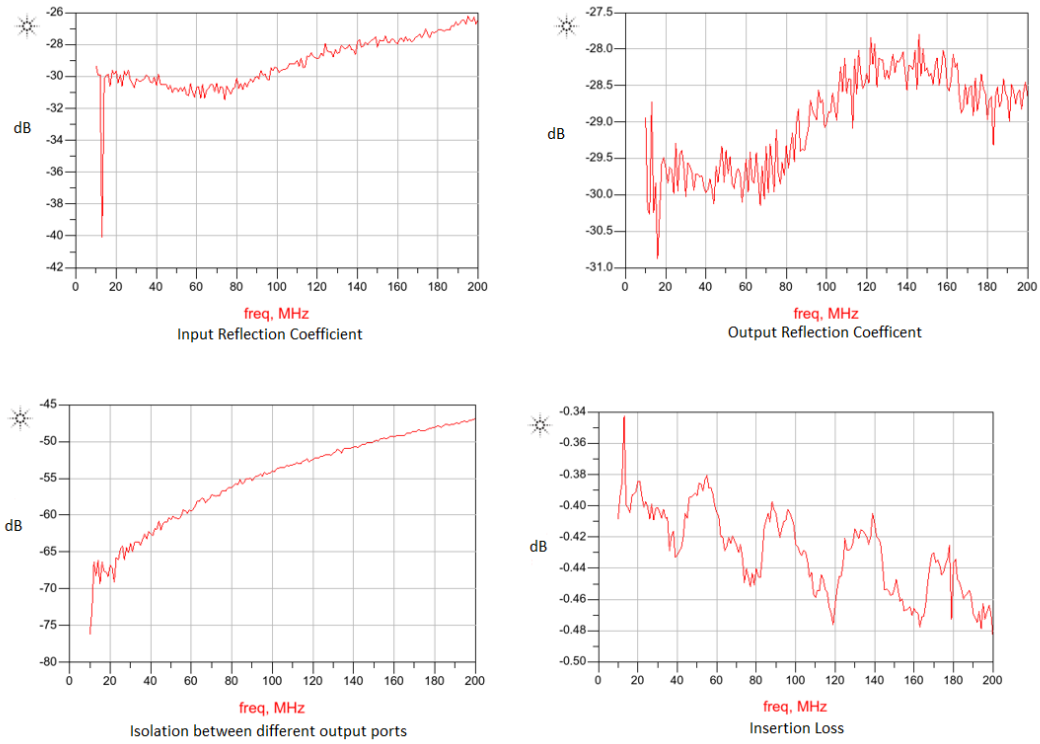

Figure 2.3 Performance of the SP6T Switch based on Evaluation Board

The SP6T and SPDT switches require digital logic for the switch to operate. These can be obtained from the digital logic pins from the PC104 connector used in cubesats for stacking up different PCBs (details of the PC104 board are discussed in the Board Design section of this chapter). Since this is a prototype board, the PC104 connector will not be implemented as that would add to the complexity of the design. Instead header pins will be used to provide the proper digital logic. The SP6T is controlled using three digital control pins and the SPDT switch is controlled by one digital control pin.

2.2 Amplifier

The signal received at the input of the receiver through the antenna will be very weak and can be expected to be as low as -90dB assuming there is negligible RFI in space. This signal must be amplified before it is filtered and processed so that the data to be extracted from the signal is not lost in noise and interference. The switching stage is therefore followed by an amplifying stage. The signal goes through further amplification in the back-end electronics. The amplification therefore does not have to be very high in the front-end electronics. For this design we will be targeting the same amount of amplification as the EDGES front-end electronics provides, which is around 40dB [39]. We would want this amplifier to be low noise. The input match also should be as low as possible so that the multiple reflections between the antenna and the amplifier due to mis-match are as little as possible. If these reflections are strong, they can manifest in the signal of interest at the output of the. The uncertainties due to these reflections will have to be accounted for. This is done in the EDGES receiver using Monte-Carlo simulations [19]. We will try to achieve very low input reflection loss in the frequency range of 50MHz – 100MHz, the frequency range between which the flattened absorption profile has been detected [40].

An amplifier that has specifications as close to the required specifications is PHA-13LN+ by Mini-Circuits. It provides gain of about 23dB, Noise Figure of 0.9dB and input reflection coefficient of about -15dB [41]. To achieve the required gain two of these amplifiers will be cascaded. To improve the input reflection coefficient further a matching network will be implemented before the amplifier.

The performance of the amplifier based on the S-parameters provided by Mini-Circuits in the frequency range of 10MHz-200MHz is plotted below. The results were obtained by simulating the S-parameters in ADS test-bench.

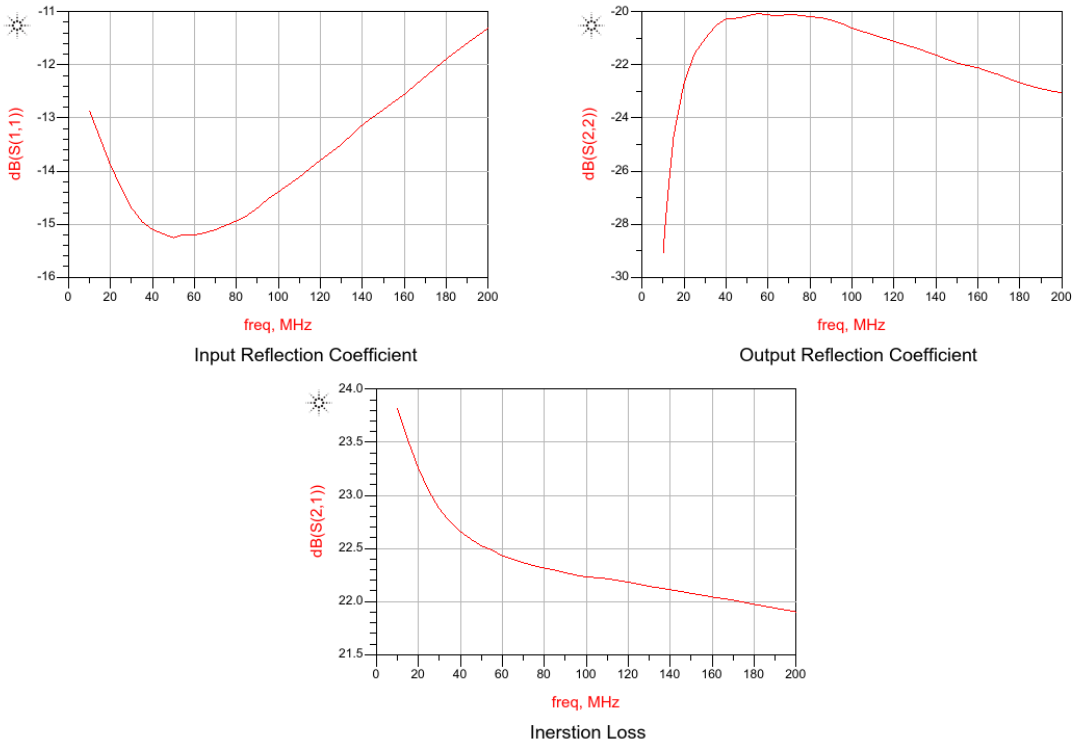

Figure 2.4 Performance of the PHA-13LN+ Amplifier

Plotting the input reflection coefficient on the Smith Chart we can see the input impedance is slightly capacitive. We add an inductor in series and tune the value to get good input match. The results after tuning the inductor are as shown below.

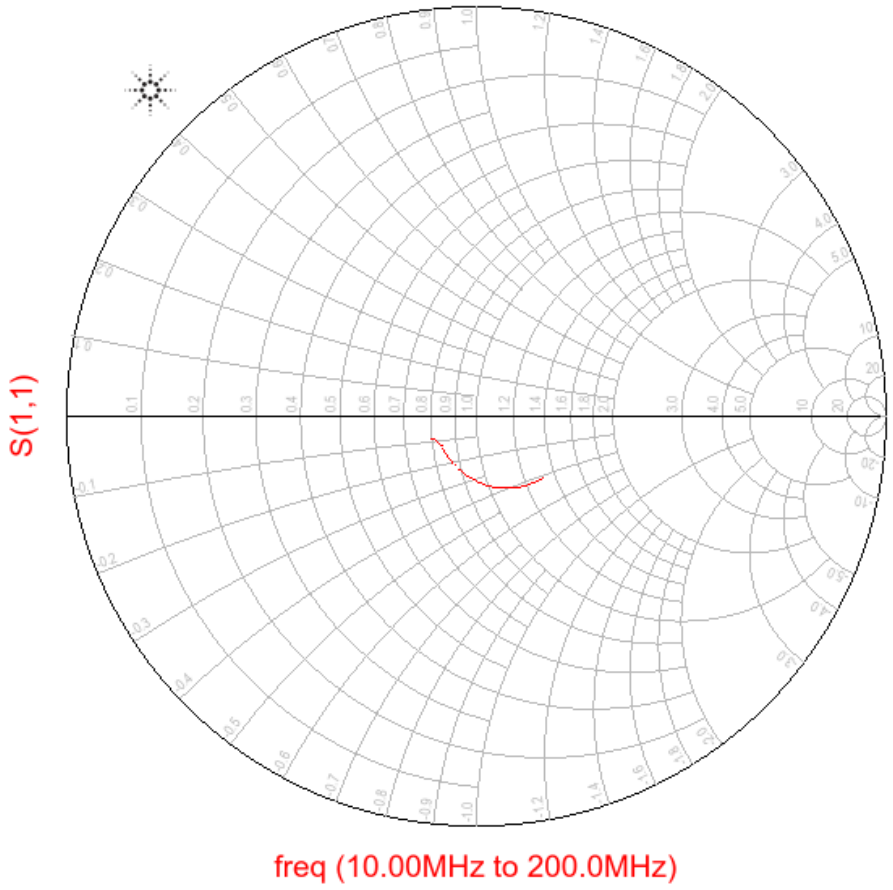

Figure 2.5 Input Reflection Coefficient on the Smith Chart

The amplifier was biased as shown in the figure below.

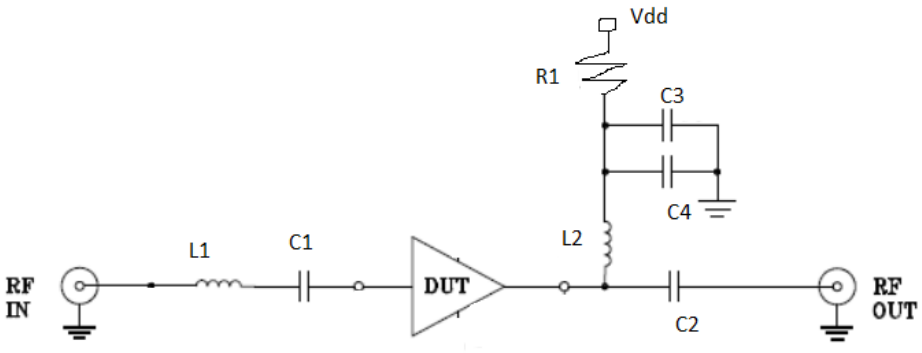

Figure 2.6 Bias Circuit of the amplifier

L1 is the input matching inductor, C1 and C2 are DC blocks, C3 and C4 are decoupling capacitors, L2 is the RF choke and R1 is the current limiting resistor.

A two-stage amplifier without the input matching inductor was built in the lab. The results obtained from this amplifier are plotted below.

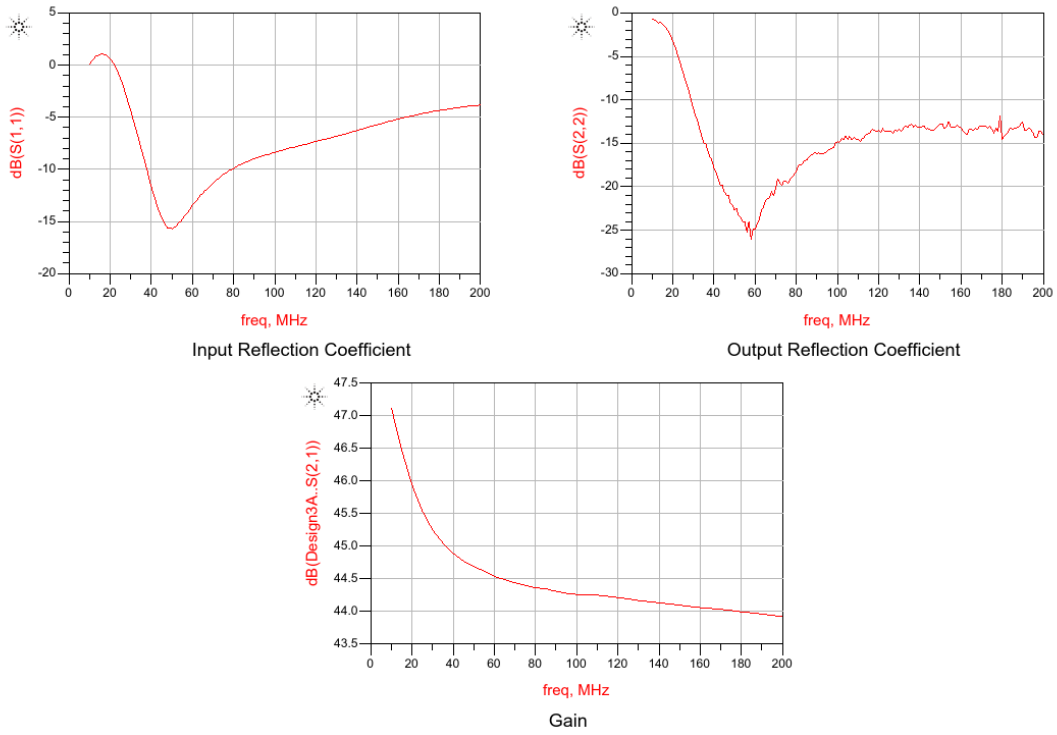

Figure 2.7 Performance of the Amplifier built in the lab

This amplifier was tested for noise figure as well which is as plotted below.

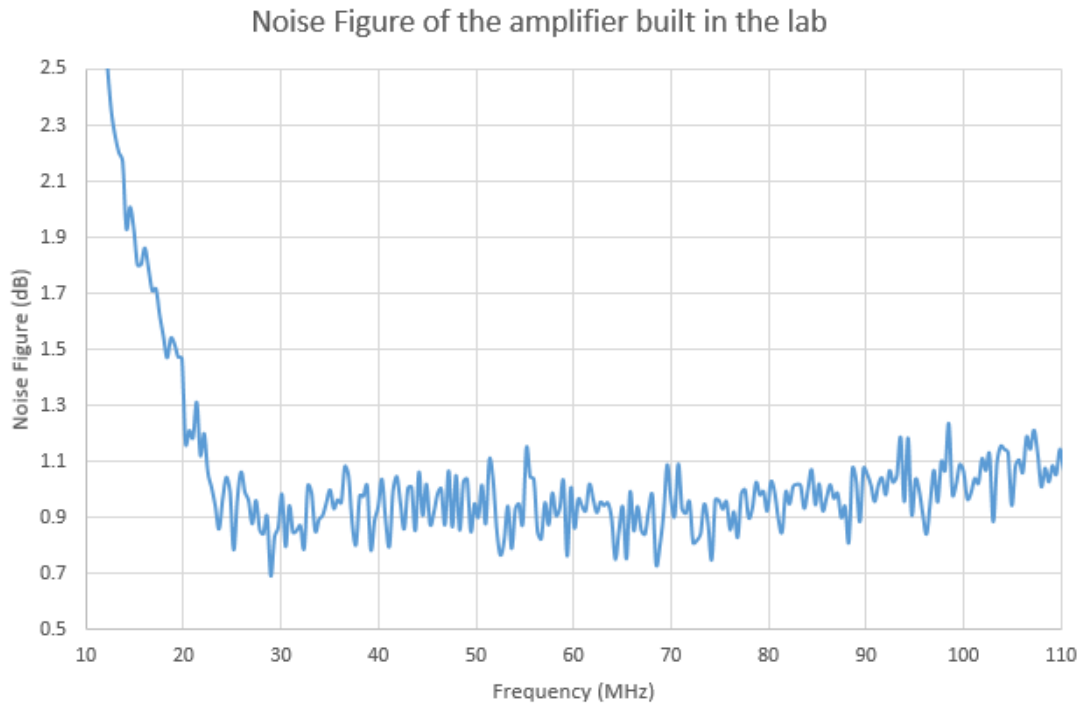

Figure 2.8 Noise Figure of the amplifier built in the lab

We can see from this data that the Noise Figure of the 2 PHA-13LN+ amplifiers cascaded gives a noise figure close to the value provided in the datasheet. The very negligible added noise could be accounted to the input trace and the losses due to the biasing circuit.

2.3 Filter

The PHA-13LN+ amplifier provides good amplification up to 1GHz of frequency. We do not want the signal above 110Mhz to be propagated beyond the front-end electronics. We add a low pass filter after the second stage of amplification to remove unwanted signals. Since we have two stages of amplification, we can tolerate a certain level of insertion loss in the filter, but we would want the signal to have a sharp cut-off as close to 110MHz as possible and high attenuation above 110MHz. As we are so low in frequency lumped component filter will be able to meet these requirements.

We choose SALF-116+ by Mini-Circuits. Simulation results of the S-parameters of the from Mini-Circuits are plotted below.

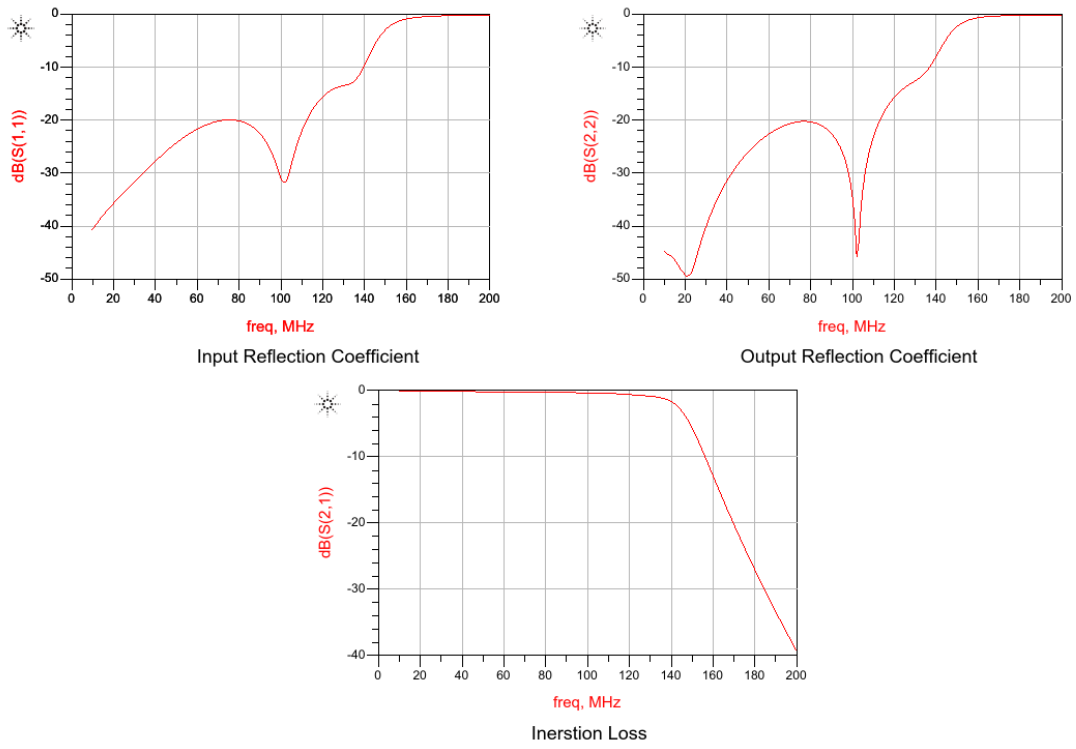

Figure 2.9 Performance of the Filter

2.4 Attenuator and Zener Diode

The EDGES LNA in the field switches between the antenna, a load which is a 30dB attenuator and the load along with the noise source which is a Zener diode every 13 seconds [19]. Similar load and noise source will be used in the new design. A diose is chosen as a noise source as it is wide band. For the Zener diode the part MMBZ523BLT3G from ON Semiconductor was selected due to its ability to handle high power (up to 225mW [42]) high Zener Voltage Range of up to 91V [42]. For the attenuator, the flatness of the attenuator and its bandwidth of operation were considered. The LAT-30+ from Mini-Circuits provides great performance in these aspects.

2.5 Simulation of entire receiver chain

The receiver from the antenna to the output of the filter was simulated using the S-Parameters provided by the manufacturer and the input matching inductor was also added in this circuit. The results are as plotted below.

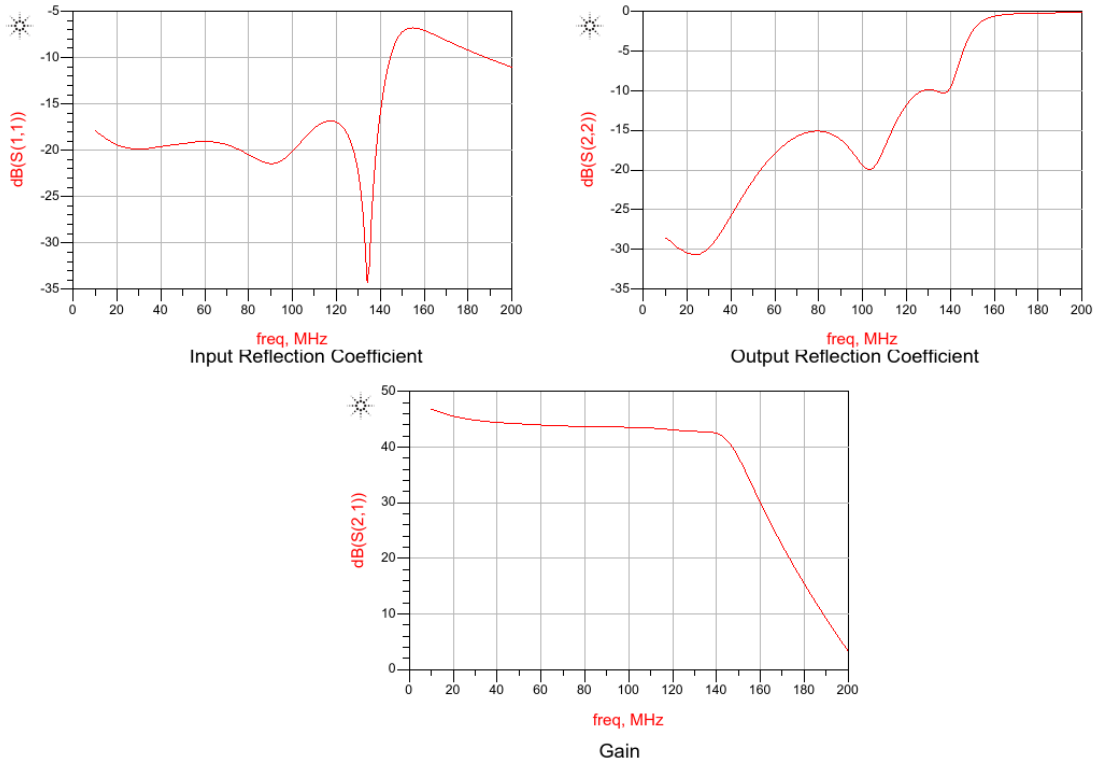

Figure 2.10 Gain and Input and Output Reflection of the complete receiver chain

2.6 Board Design

The size of the board is that of a standard Printed Circuit Board (PCB) for a cubesat. Cubesats use PC/104 connectors for stacking up multiple PCBs to make the compact size of the satellite possible while having the ability to perform multiple functions. The PC/104 connector provides different voltage levels required to power the board and have different digital outputs to control the components on the board.

Since this is a proto-type board for only the front-end receiver of the EDGES program the entire PC/104 will not be implemented. Header pins will be used instead to provide the control signals and power for the components in the design. The design however will be implemented on a PCB that meets the dimension specifications of the PC/104 board to ensure that it can be implemented in the space provided. The PC/104 dimensions are shown in the figure below.

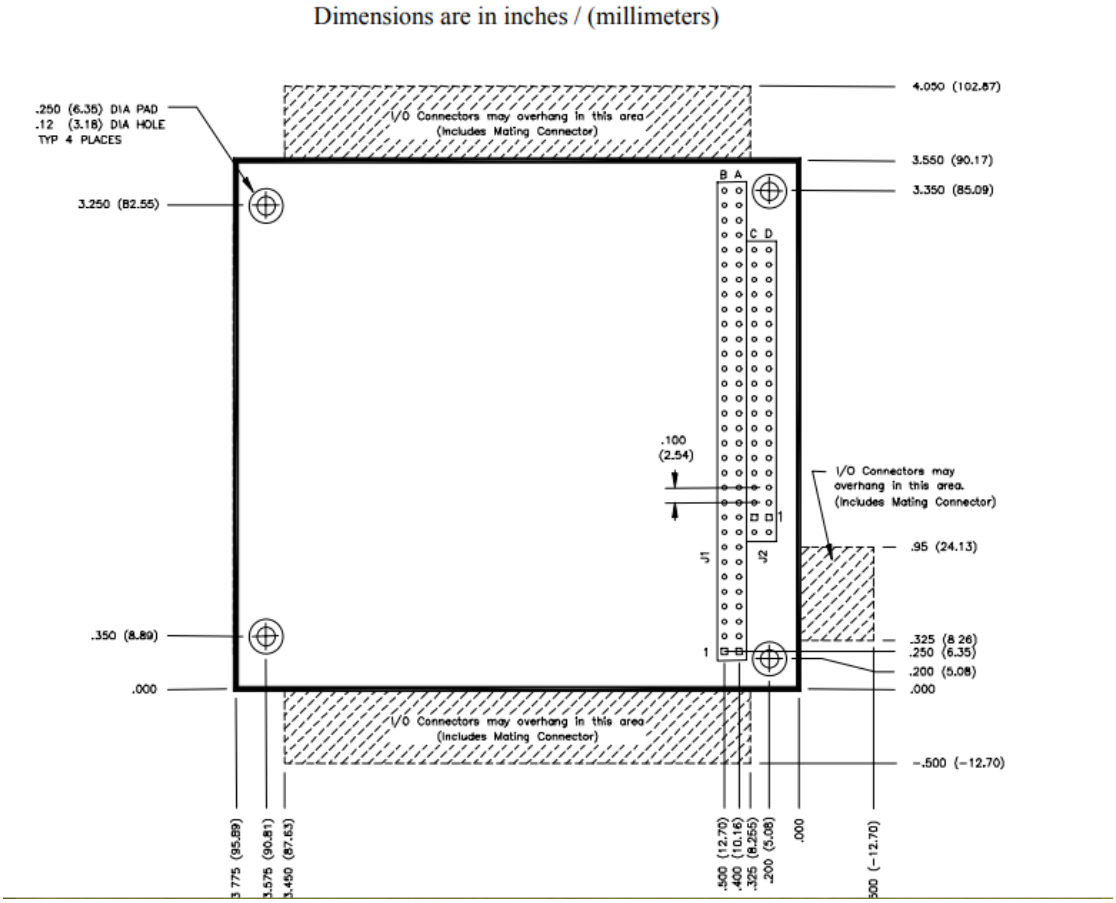

Figure 2.11 Mechanical Dimensions of the PC/104 [43]

When designing a PCB for cubesat the material to be used as the dielectric between the different copper layers must be considered carefully as the outer space can have different effects on different materials. One such effect is outgassing, which is the release of gas trapped within the material. This can degrade the performance of the circuit built on these PCBs. The Rogers TMM series material and RT/Duroid materials

present good performance for space applications [44]. Despite the great performance of these materials we will be using FR4 material for our design due to cost constraints.

Having decided the material of the board, the next step would be figuring out the transmission media for the design and using the properties of the material to find the dimensions of the transmission media. The available choices for the transmission media are microstrip, stripline and grounded co-planar waveguide (GCPW). The option of stripline can be eliminated due to the complexity required to design a PCB with surface mount components using stripline. Microstrip is easy to implement on a PCB but a GCPW provides less variation in characteristic impedance for a wide range of frequencies [45]. The ground of the GCPW can also be used to increase the shielding between different signal lines which in turn can help improve isolation between different ports of the receiver. Due to these reasons GCPW will be used as the transmission media despite the slightly increased complexity in the design.

To find the width of the transmission line and the spacing between the line and the ground plane, the LineCalc tool of the Advanced Design System (ADS) Software by Keysight Technologies was used. The software allows for a CPWSUB component to be added to the schematic. In this component all the properties of the FR4 material, the thickness of copper and the dielectric material were added. Then a GCPW component was added. The substrate along with the GCPW was added to the LineCalc tool. The LineCalc tool then allows you to calculate the gap and width in mils for a given characteristic impedance. The results for 50Ω characteristic impedance are shown in the image below.

Now we have all the necessary information to move forward with the layout of the board. The layout was done in KiCad Software. We started off by creating the

footprints for all the components finalized for the design. The next step was to place the footprints of the components to make the routing easier while ensuring good placement from the RF performance perspective. First the SMA connector for the input of the receiver i.e. the antenna and the SMA connector for output of the receiver i.e. the output of the filter was placed on opposite ends. This was done to ensure that the signal from the antenna does not enter the system after the amplifier as that can result in faulty measurements. Next, the amplifier and the attenuator were placed such that the signal lines for them were orthogonal to each other. The components were placed to avoid the bending of signal lines as much as possible. The DC power lines and digital control lines were placed next to each other on one end of the board. All the power lines and the digital lines were routed on the back-copper layer of the board, while the RF lines were routed on the front copper layer. Two layers of ground were added in between the front and back copper layer to improve shielding between RF and digital lines making the board of total four layers. To provide consistent ground performance vias were added throughout the board.

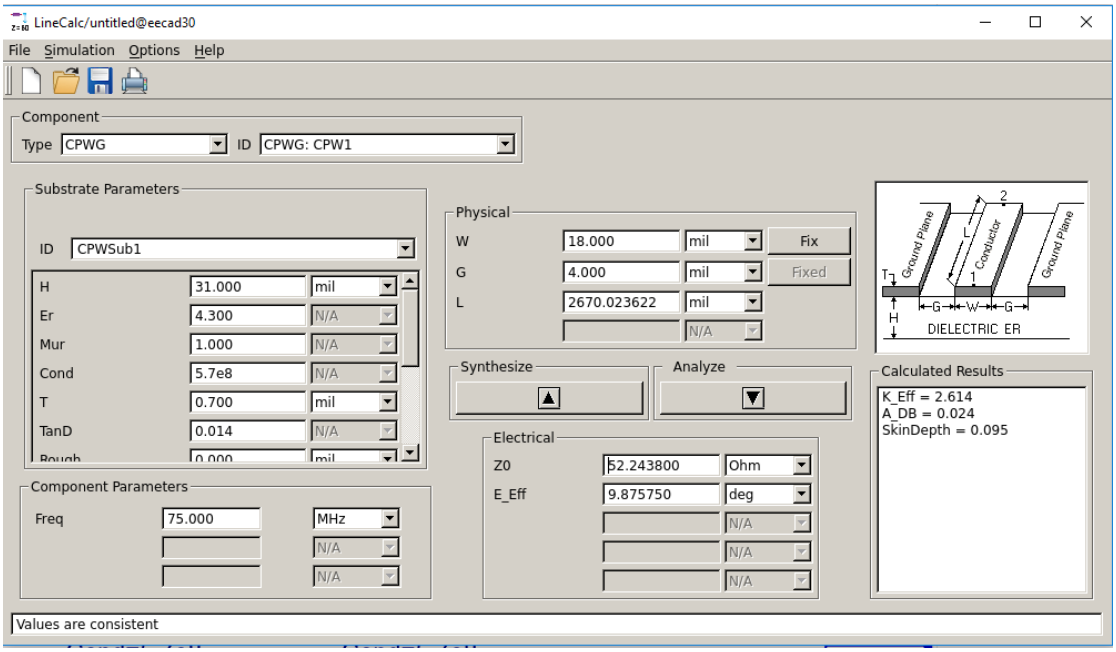

Figure 2.12 Calculation of the width and gap for the GCPW

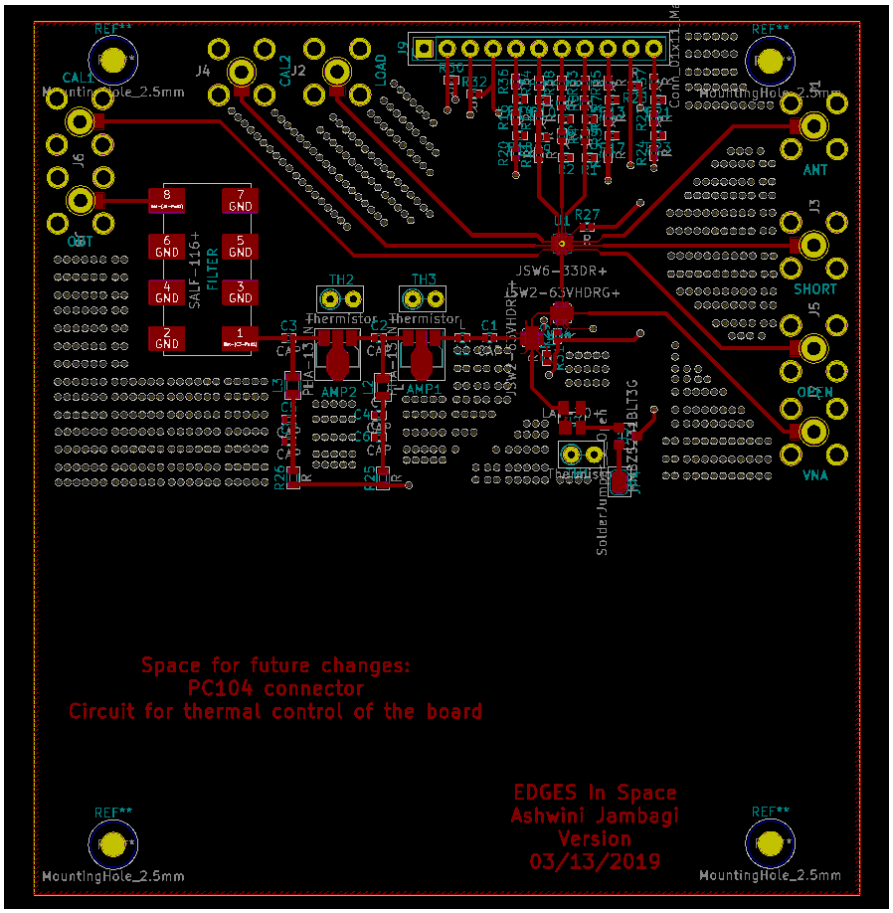

Figure 2.13 Front Copper Layer of the board

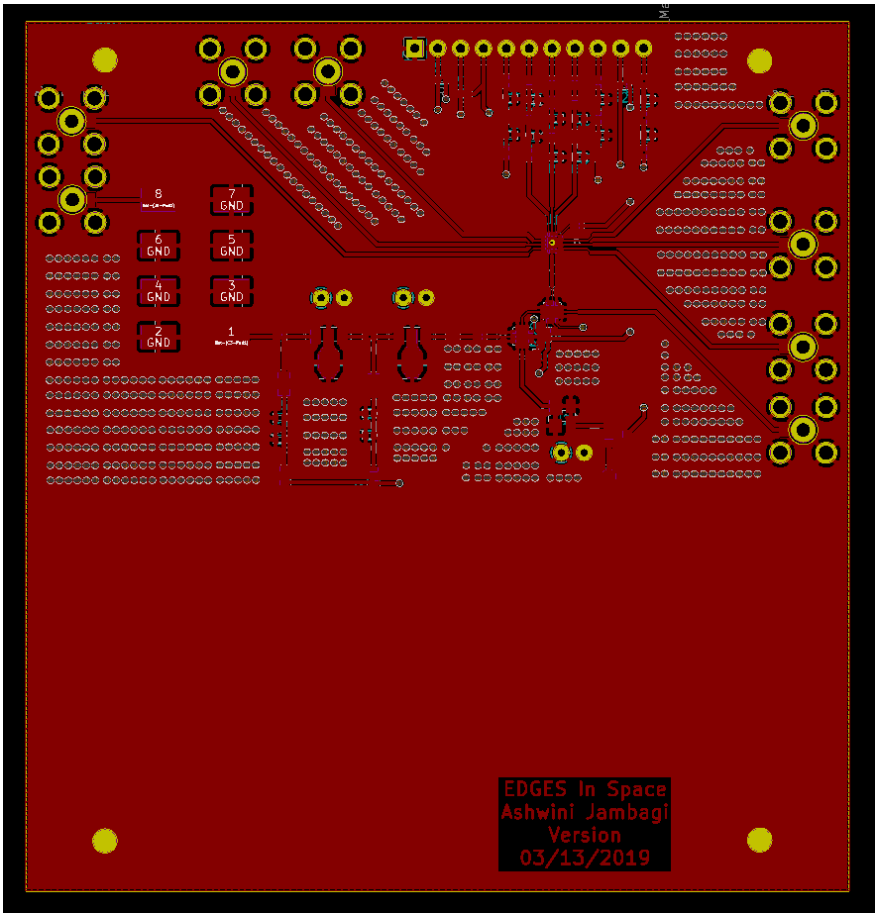

Figure 2.14 Front copper layer of the board with ground shielding

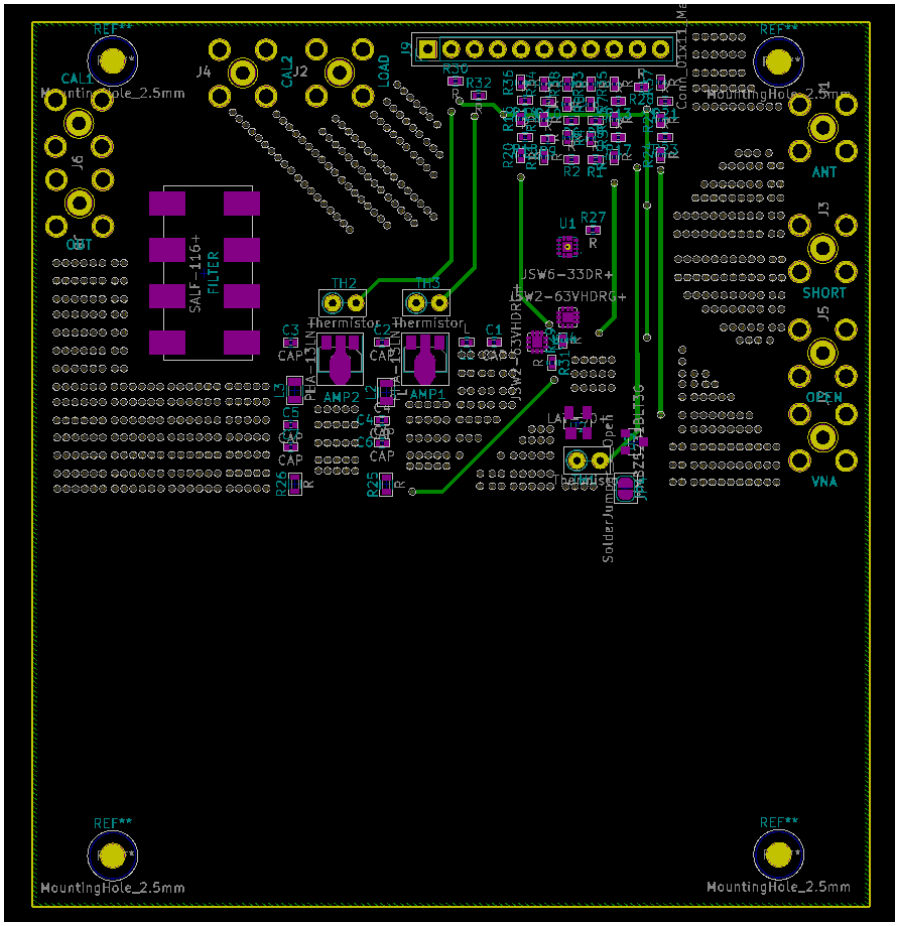

Figure 2.15 Back Copper Layer of the Board

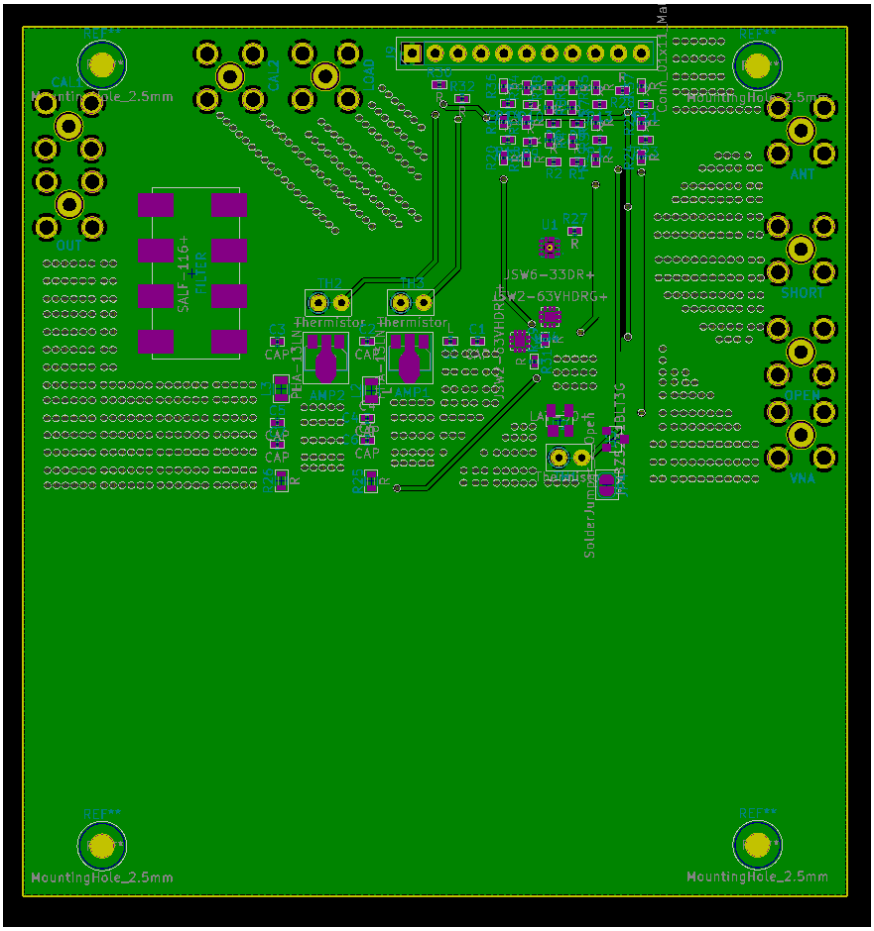

Figure 2.16 Back Copper Layer of the board with ground shielding

The inner layers i.e. the layers 2 and 3 are not shown here as they are just plain ground layers of copper.

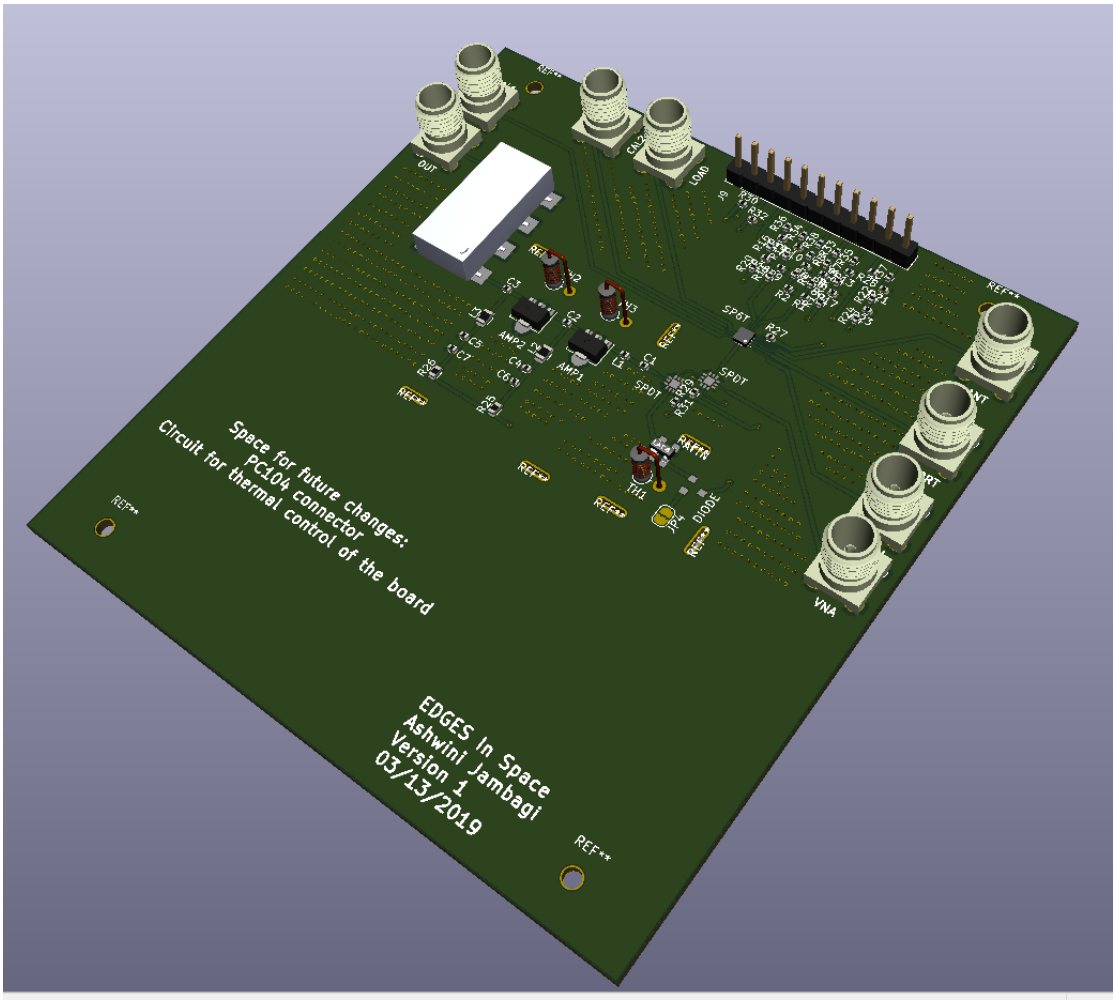

Figure 2.17 3D view of the board generated by KiCad

CHAPTER 3

TUNING AND OPTIMIZATION

Once the PCB was printed, the board was assembled by soldering the components. An image of the final assembled board is shown below.

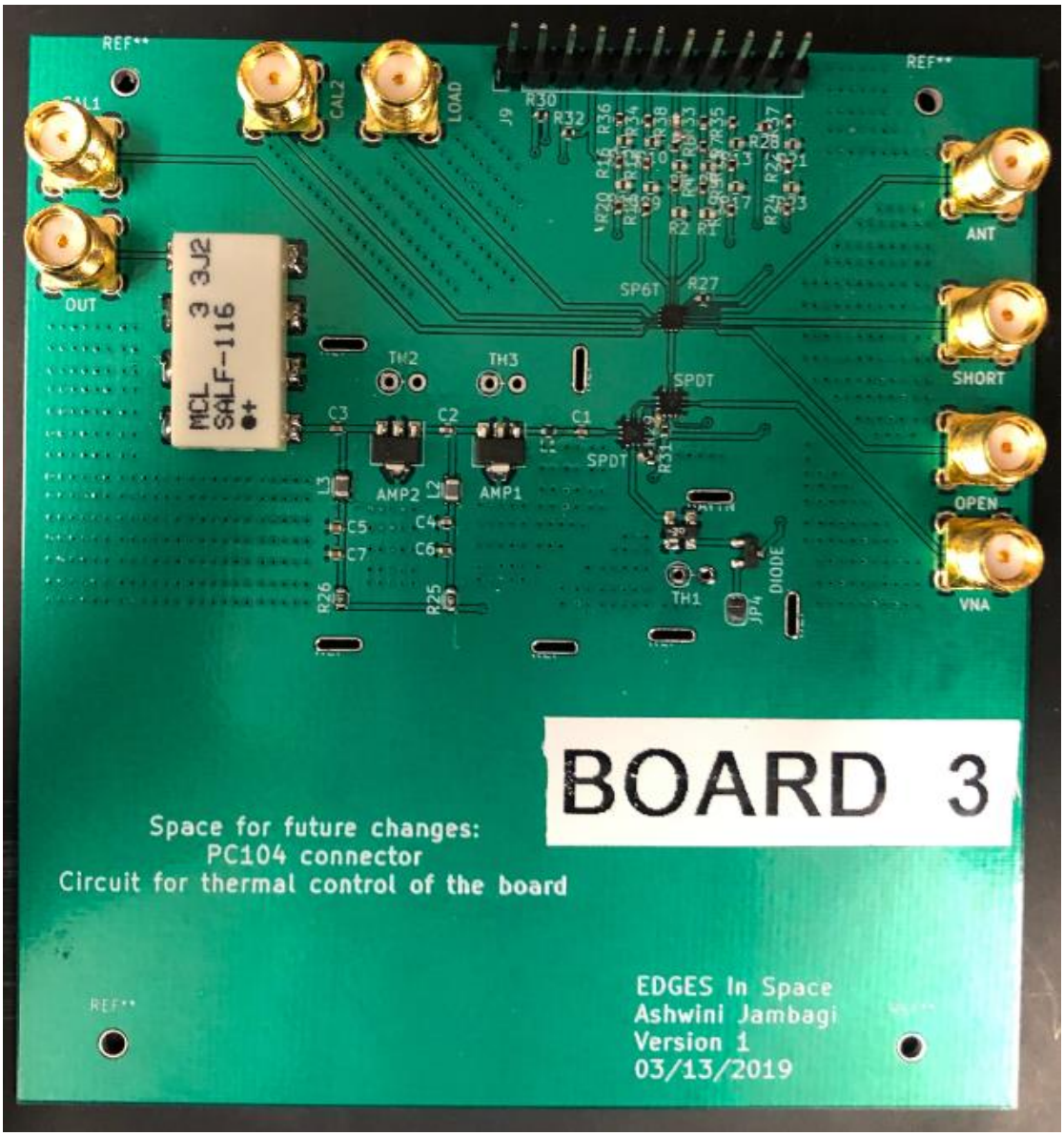

Figure 3.1 Final assembled board

Power was supplied to this board and the proper control logic was provided to enable the switches so that the amplifier was connected to the antenna. The S-

parameters of the board were recorded for this configuration. The details of the test procedure and the S-parameters are provided in Chapter 4. Here only S11 of the board is shown.

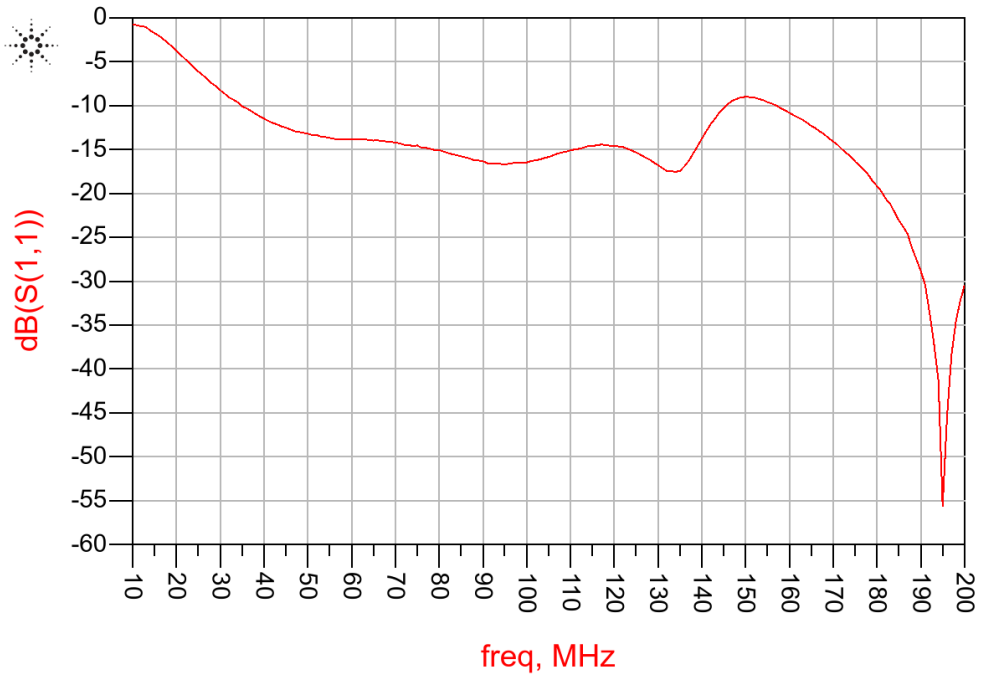

Figure 3.2 Measured S11 of the path from antenna to output with 15nH input matching inductor

We can see that in the frequency range of interest we measure a S11 of about -15dB. We are going to tune the input matching inductor and see if we get a better S11. Based on the simulations we found that an inductor value of 15nH provided good S11. We will start by going lower on this value as the traces might add parasitic inductance.

We start by going one value lower i.e. 12nH. For this value the S11 we get is plotted below.

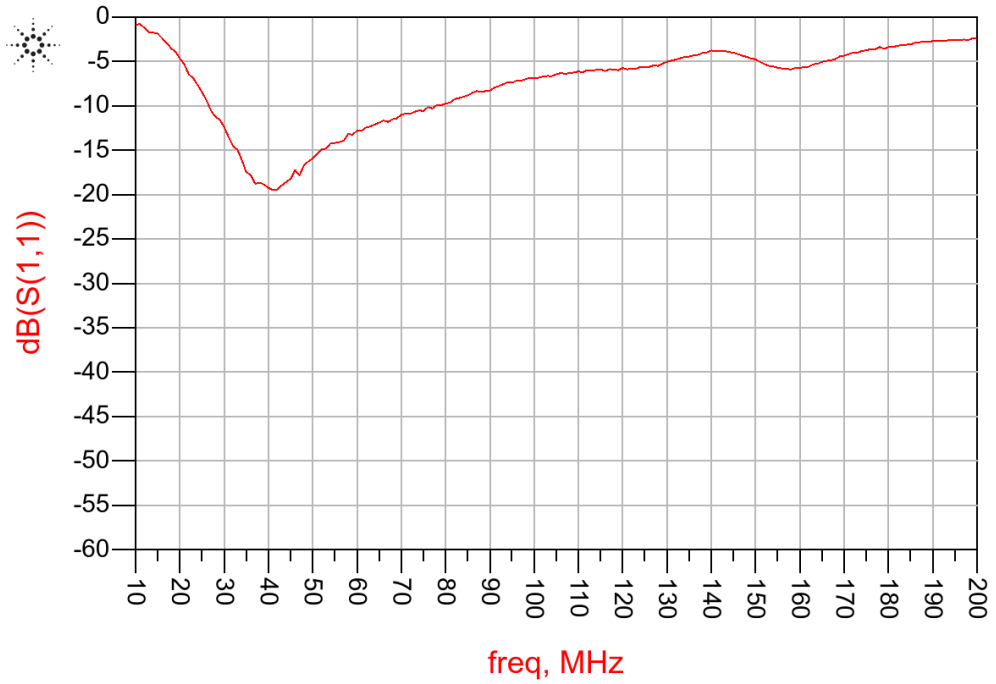

Figure 3.3 S11 of the path from antenna to output with 12nH input matching inductor

Since this value didn't help, we will try going lower by one more value to ensure lower inductance is not desirable. We use the value 8.2nH. The S11 for 8.2nH input matching inductor is as plotted and we see that this value does not provide any improvement either.

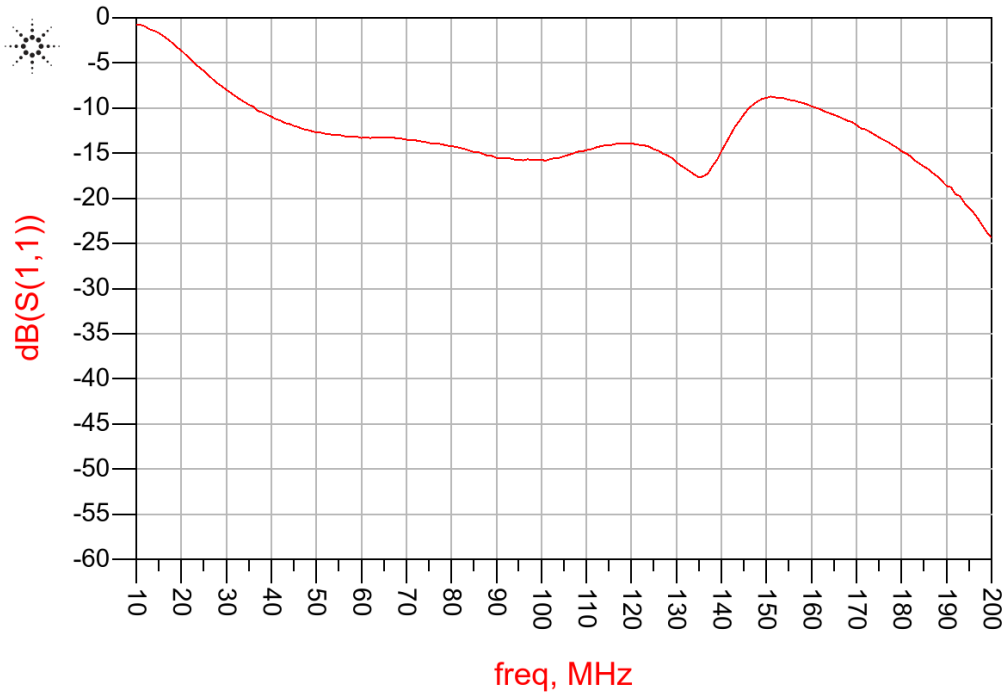

Figure 3.4 S11 of the path from antenna to output with 8.2nH input matching inductor

We see that going lower in the inductor value is not helping. We try by increasing the inductor value. We go one step higher that 15nH i.e. 18nH and plot the S11 which is shown below.

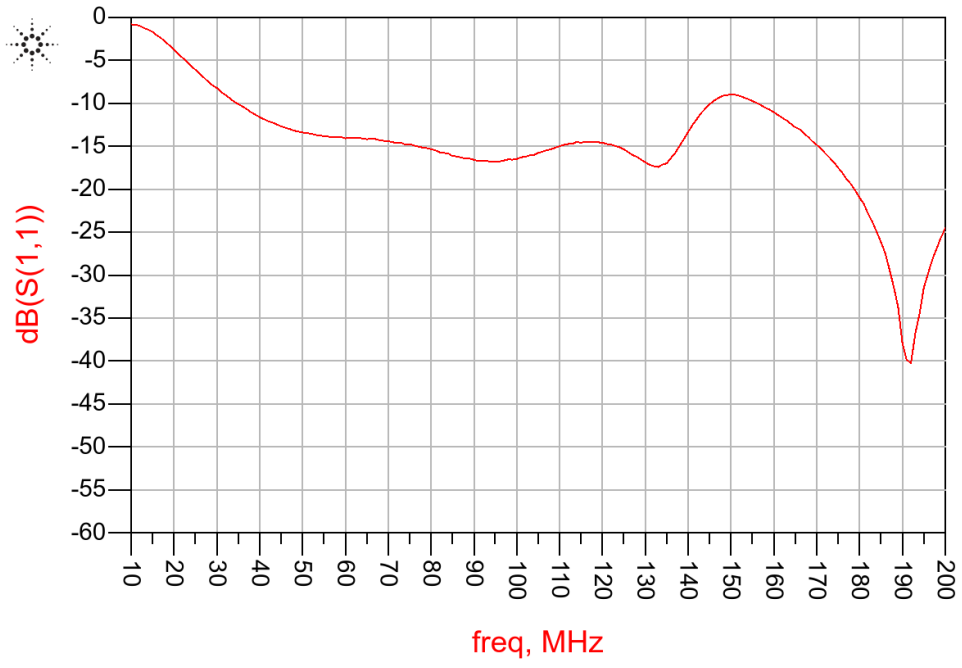

Figure 3.5 S11 of the path from antenna to output with 18nH input matching inductor

As this does not help either we try going one more step higher i.e. 22nH. The S11 is as shown.

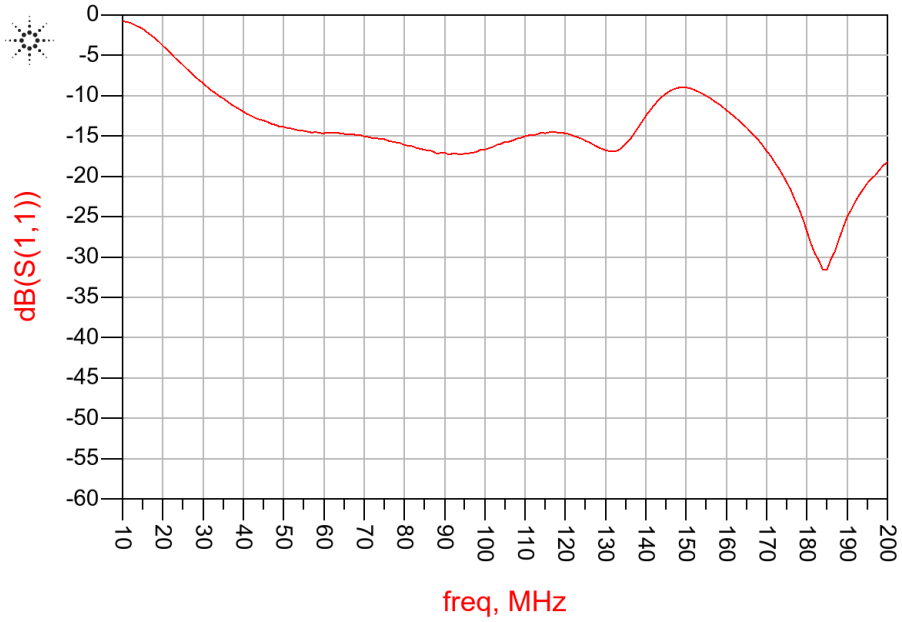

Figure 3.6 S11 of the path from antenna to output with 22nH input matching inductor

We can see from these different results that changing the value of the input matching inductor does not help much to improve the S11 of the entire system. So, for the further measurements we will continue with the simulated value of 15nH.

CHAPTER 4

FINAL RESULTS

4.1 S-Parameters

The S-Parameters of the board were measured using the Rhode & Schwarz ZVL 9kHz-3GHz Vector Network Analyzer (VNA) and Spectrum Analyzer. The calibration method of Short Open Load and Through (SOLT) was used. The setup for this measurement is shown in the image below. The power for the board was supplied using Keithley 2230-30-1 Power Supply and the temperature of the board was controlled using a thermal sensor. The results obtained have been plotted in the following sections.

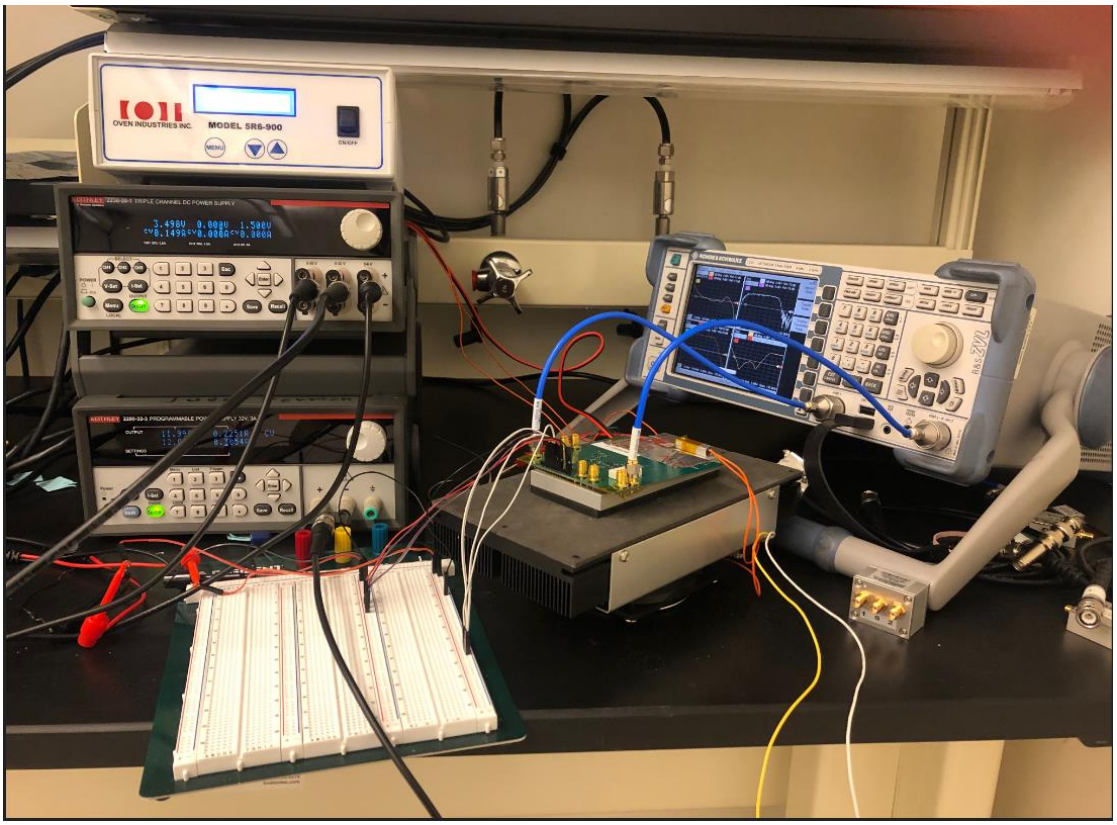

Figure 4.1 Setup for S-Parameter and Noise Figure measurement

4.1.1 Gain

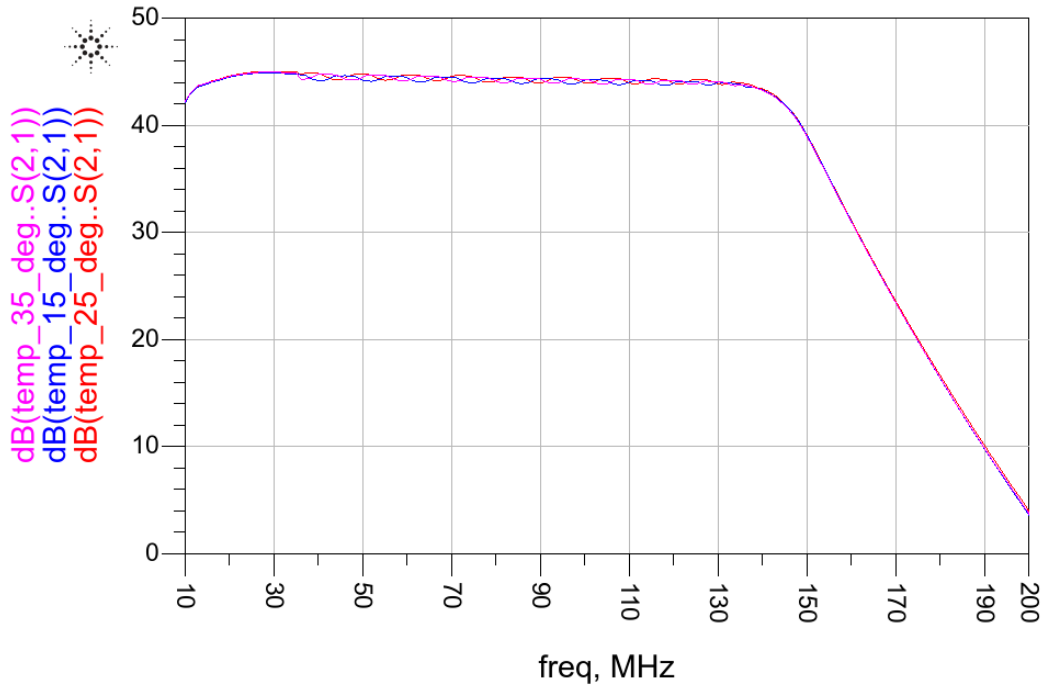

Figure 4.2 Gain of the receiver at different temperature

The gain remains steady with varying temperature.

4.1.2 Reflection Coefficient

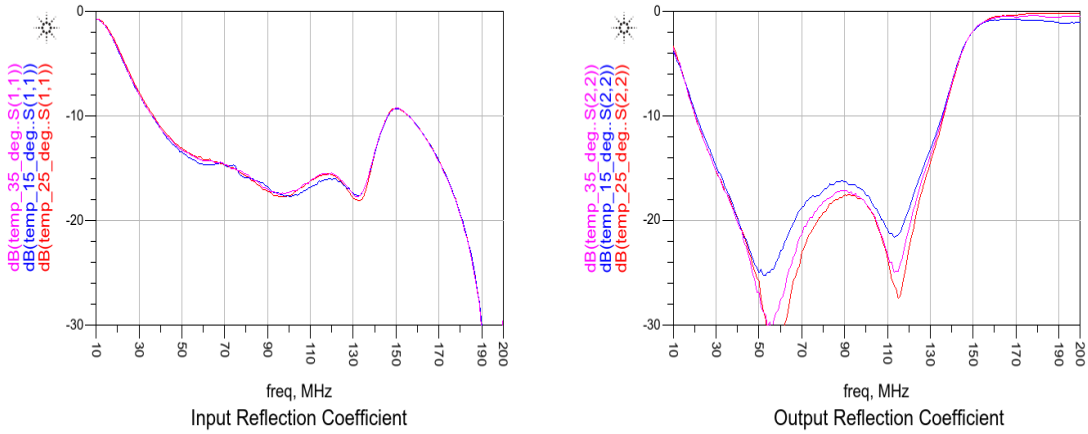

Figure 4.3 Input and Output Reflection Coefficient for different temperatures

We can see that the output reflection coefficient varies with temperature, but the input reflection coefficient remains steady. This could be accounted to the sensitivity of the filter to temperature.

4.1.3 Isolation

The isolation between the ports connected to the calibration standards when the switch connection is made to the VNA is plotted below for different temperatures.

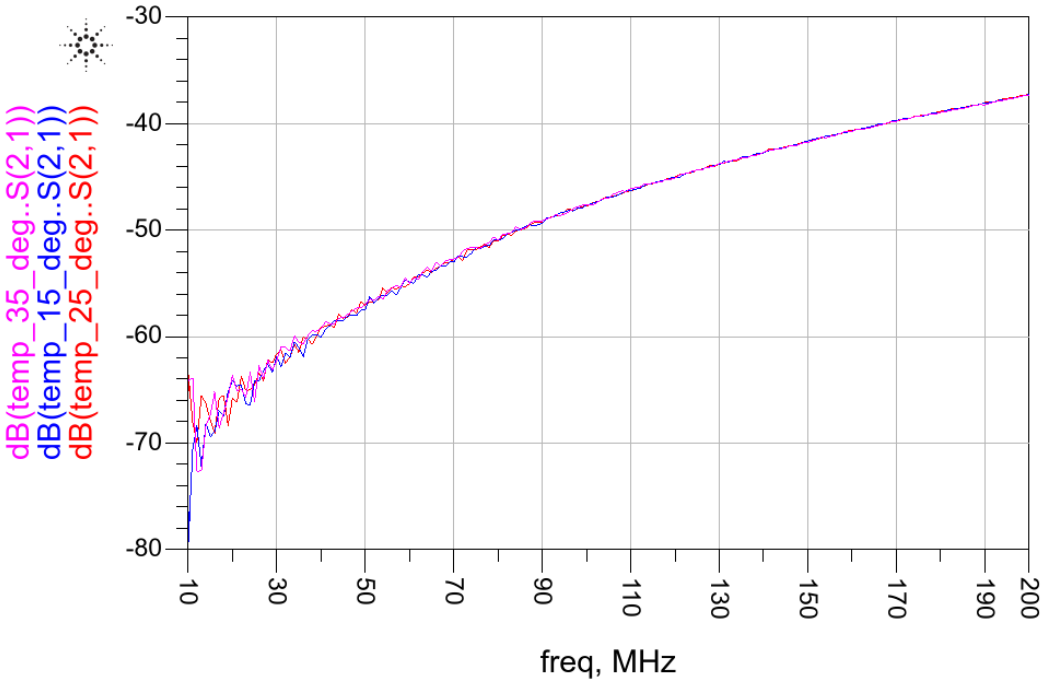

Figure 4.4 Isolation between various calibration standard ports for different temperatures

4.1.4 Insertion loss from antenna to VNA

To be able to calibrate and measure the reflection coefficient we should be able to calibrate it at the reference point where the antenna is connected. But in the board the signal goes from the antenna to the VNA through a series of switches and suffers

some loss. It is necessary to correct for this error. This loss can be calculated by measuring the Insertion loss from the antenna to the VNA when they are connected through the switches. This measurement at different temperatures is plotted below.

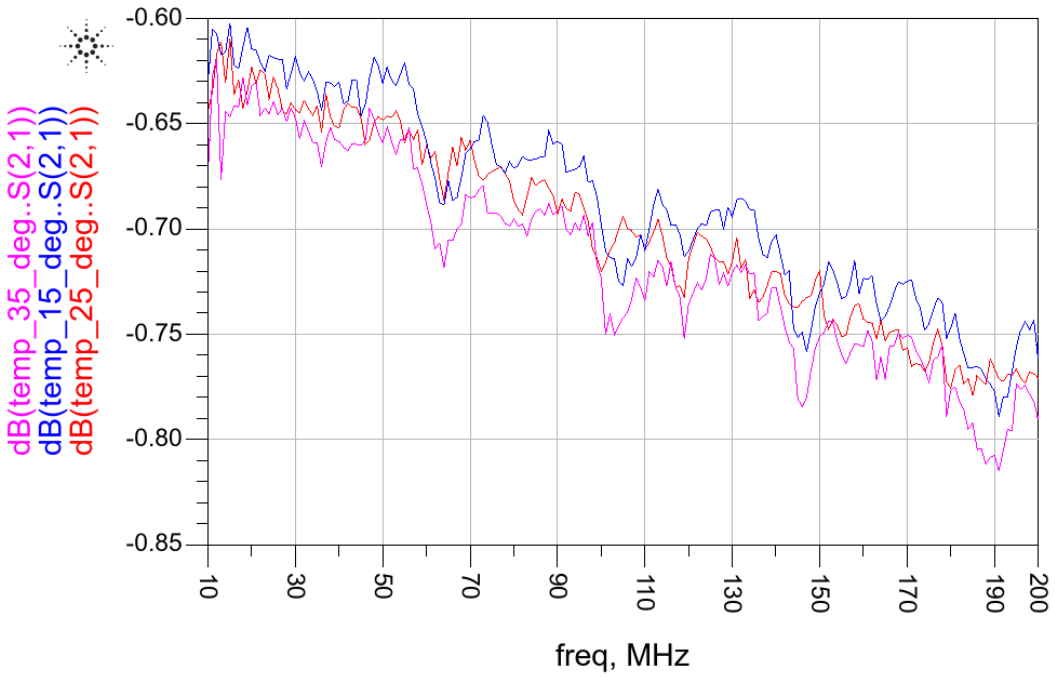

Figure 4.5 Insertion loss from antenna to the VNA port for different temperatures

4.2 Noise Figure

The Noise Figure was measured using the Y factor method. The setup for this measurement was like the measurement of the S-Parameter. The difference was that the Rhode & Schwarz instrument was used in the Spectrum Analyzer mode and the input of the board was connected to a noise source. The noise source used was the Hewlett-Packard 346C Noise Source 10MHz-26.5GHz. The spectrum with the noise source off served as the cold measurement and the spectrum with the noise source turned on was the hot measurement. The Y factor which is the ratio of the hot power and the cold power was measured. This factor was used to find the equivalent noise temperature

which was then used to find the noise factor. The noise factor converted to dB gave the final Noise Figure. The Noise Figure for different temperatures is plotted below.

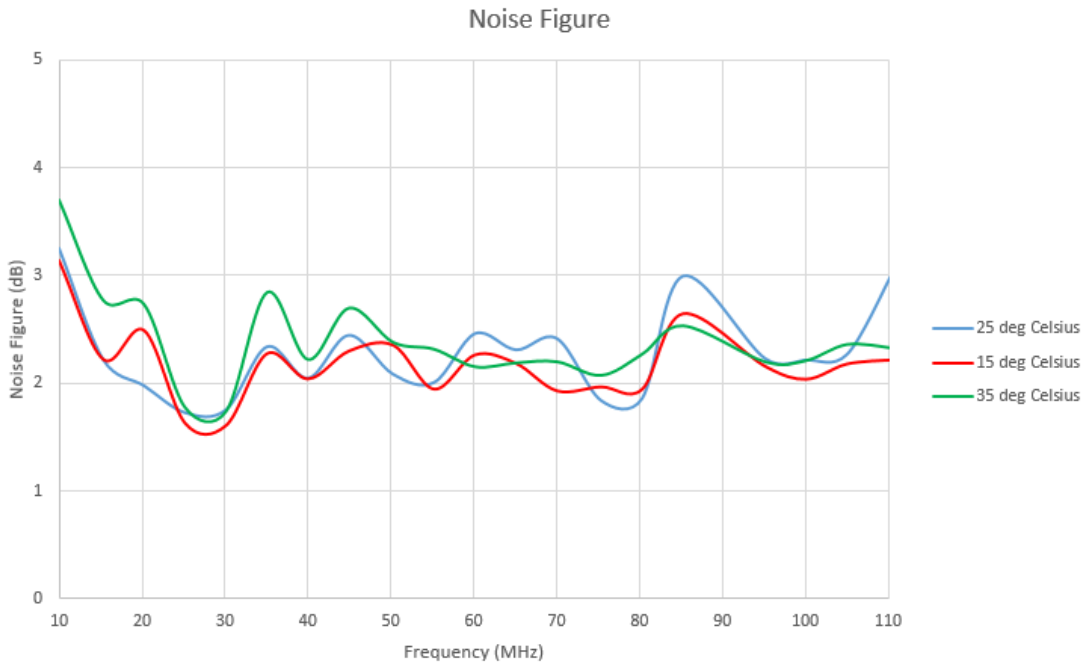

Figure 4.6 Noise Figure for different temperatures

Based on the performance of the individual components we could have estimated the Noise Figure of the receiver as follows:

Noise Figure of Receiver = Insertion loss of SP6T + 2*Insertion Loss of SDPT + Noise Figure of LNA.

Noise Figure of Receiver = 0.42 + 2*0.22 + 1 = 1.86dB

The average of the plotted noise figure is 2.2dB. The Noise Figure is 0.34dB worse than expected. But this can be tolerated. We also see that the noise figure does not vary more than 0.5dB with temperature.

4.3 Linearity

Linearity measurement of 1 dB compression point was done using the Spectrum Analyzer mode of the Rhode & Schwarz ZVL instrument. The input power of known value of frequency 75MHz (center frequency for the range 50-100MHz) was provided to the receiver and the output power was recorded using the spectrum analyzer. This data was plotted, and the expected linear behavior was plotted. The input power where the gain was 1 dB less than the expected output power was then found which gave us the 1dB compression point of the receiver. An image of the setup of this measurement is shown below.

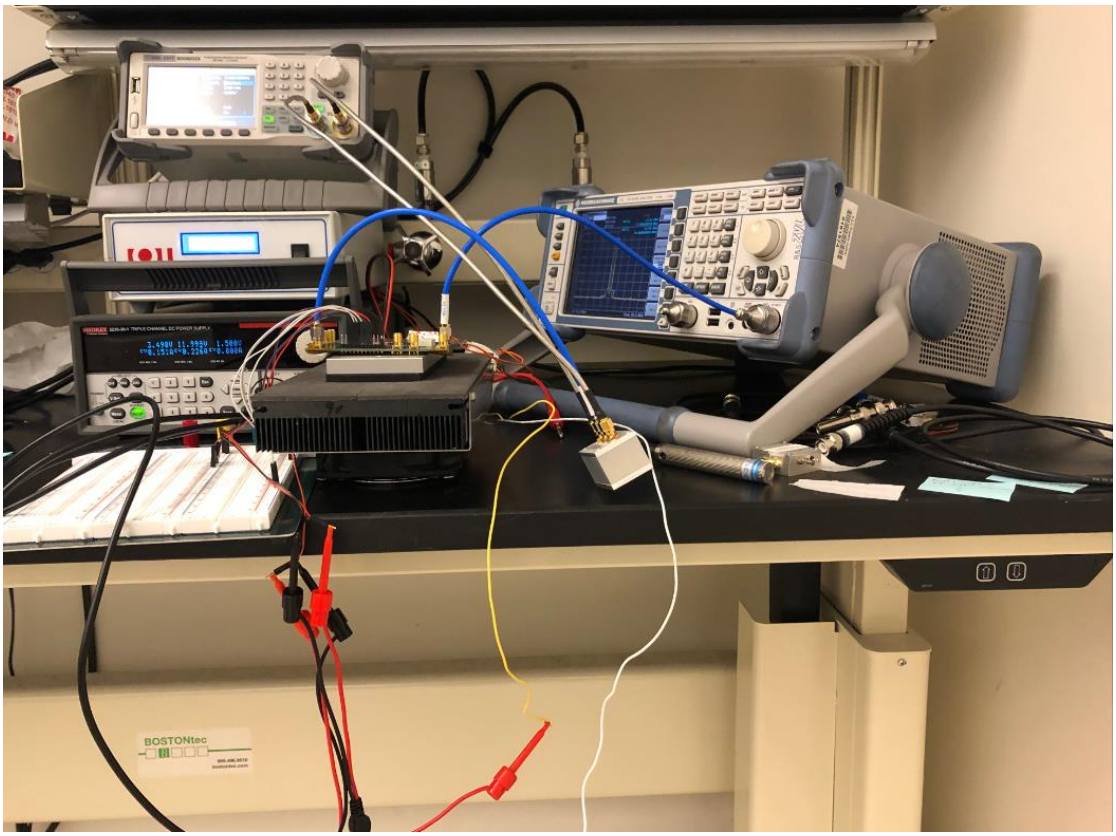

Figure 4.7 Setup for P1dB and IIP3 measurement

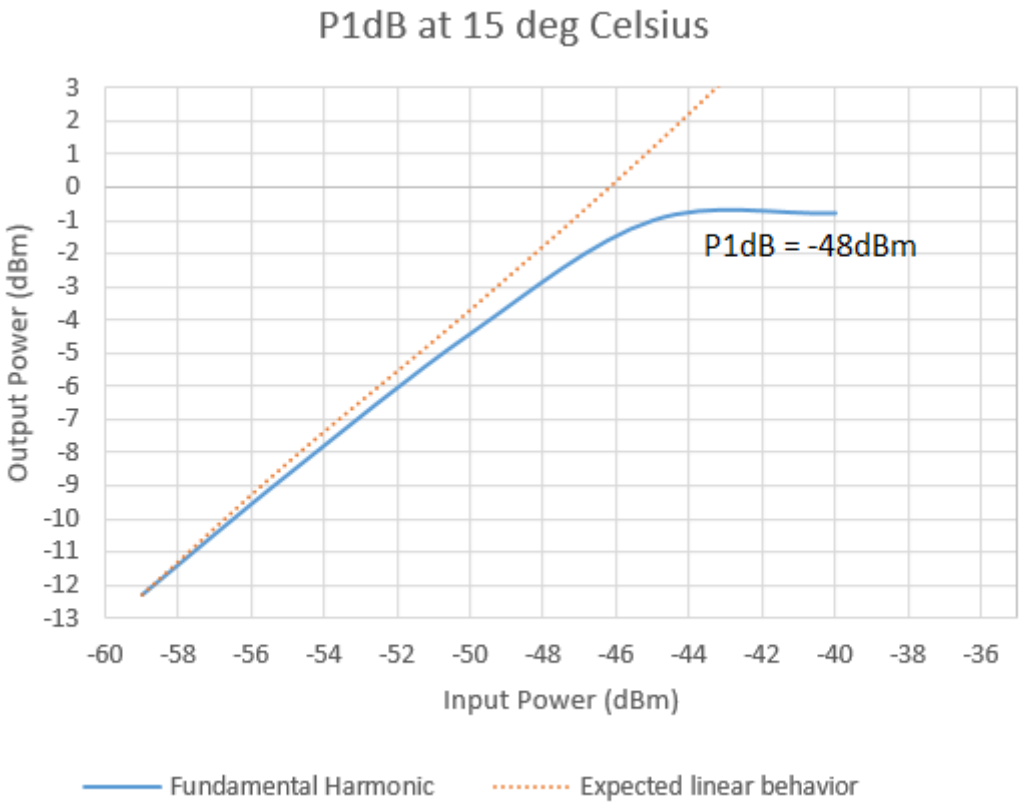

Figure 4.8 P1dB plot for 15^0C temperature

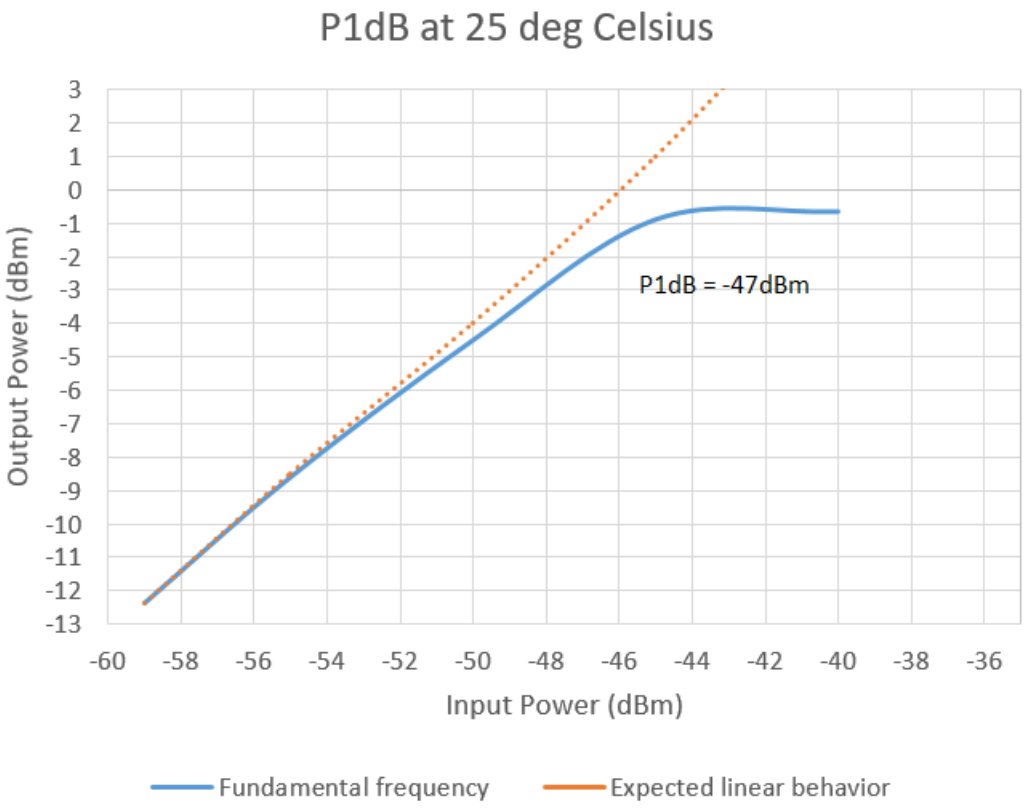

Figure 4.9 P1dB plot for 25^0C temperature

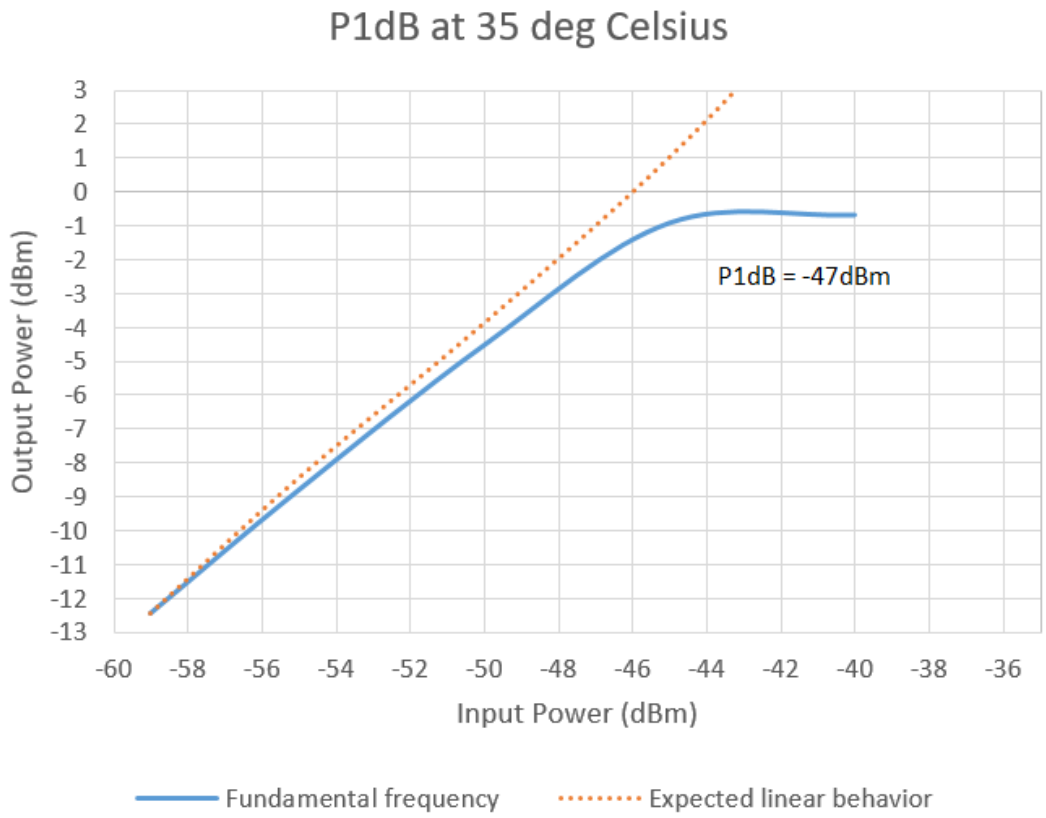

Figure 4.10 P1dB plot for 35^0C temperature

For the Input Third Order Intercept Point (IIP3) measurement signals of equal input power and of frequencies 74MHz and 76MHz were sent to the input of the receiver using a power combiner. The powers of the third harmonics of these two frequencies occurring in the pass-band i.e. 72Mhz and 78MHz were then recorded along with the powers of the fundamental frequencies. These recorded output powers were plotted against the known input powers. The expected linear behavior for the fundamental and the third harmonic was plotted and the point where the intersected was noted. The input power at this intersecting point is the IIP3. This measurement was repeated for different temperatures.

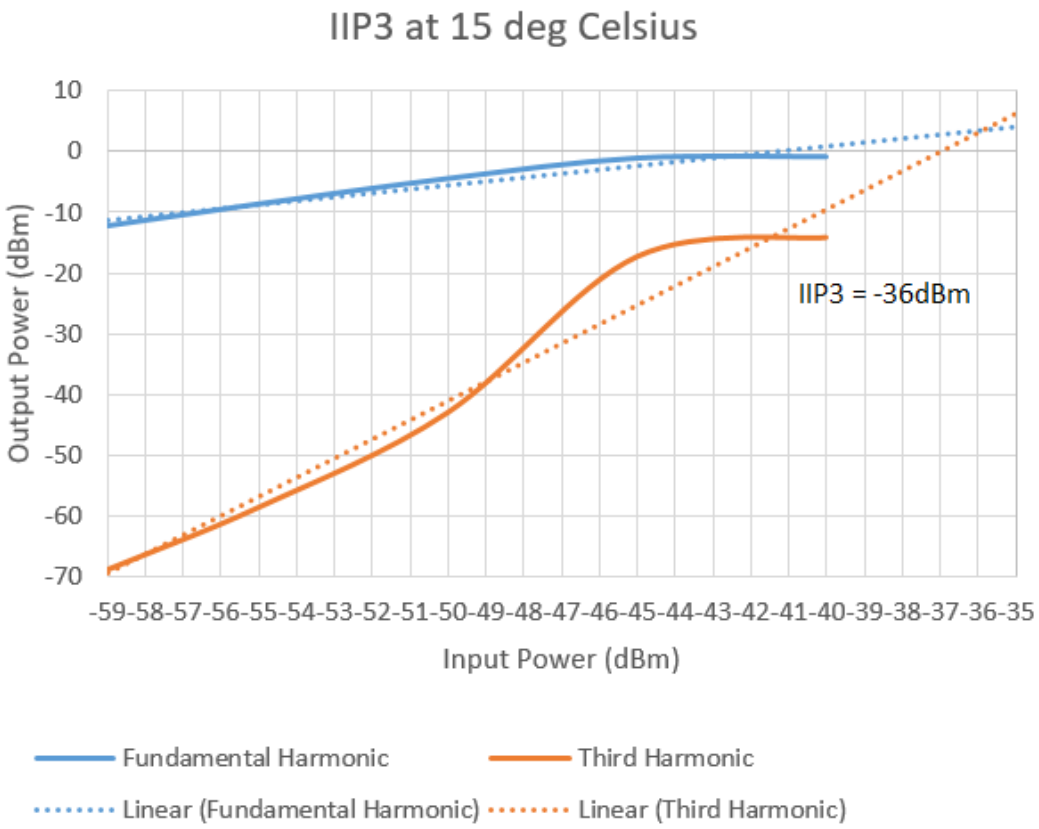

Figure 4.11 IIP3 plot for 15^0C temperature

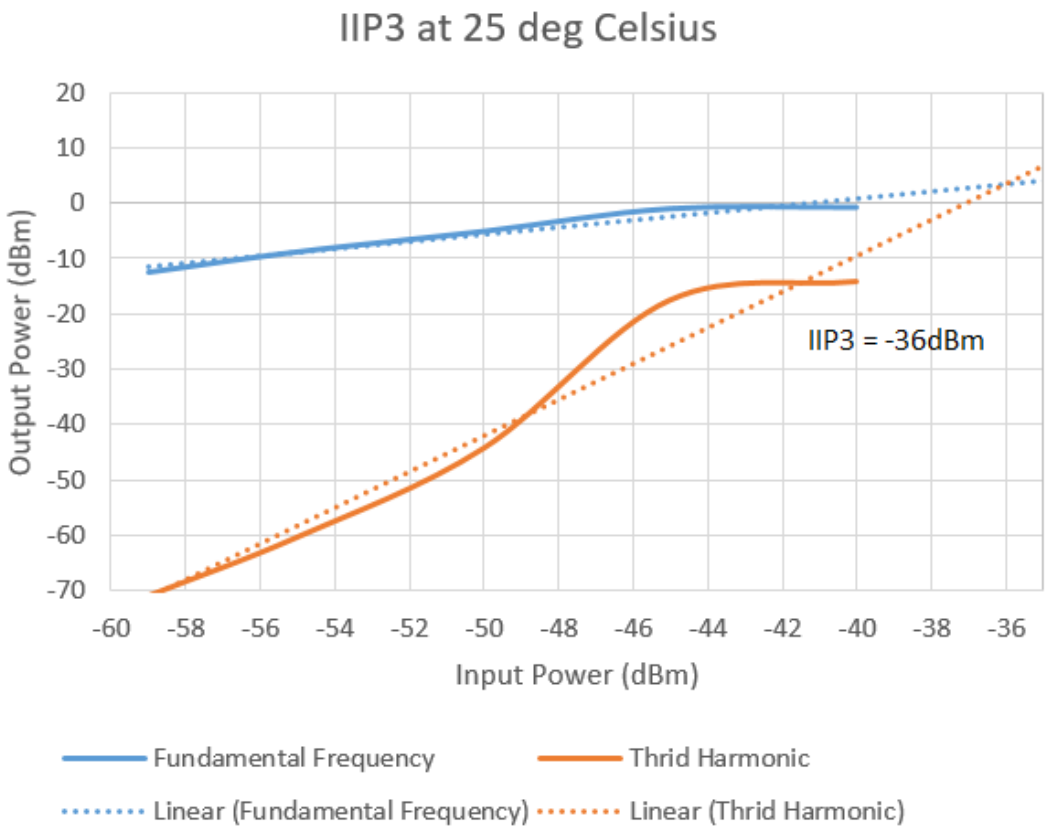

Figure 4.12 IIP3 plot for 25^0C temperature

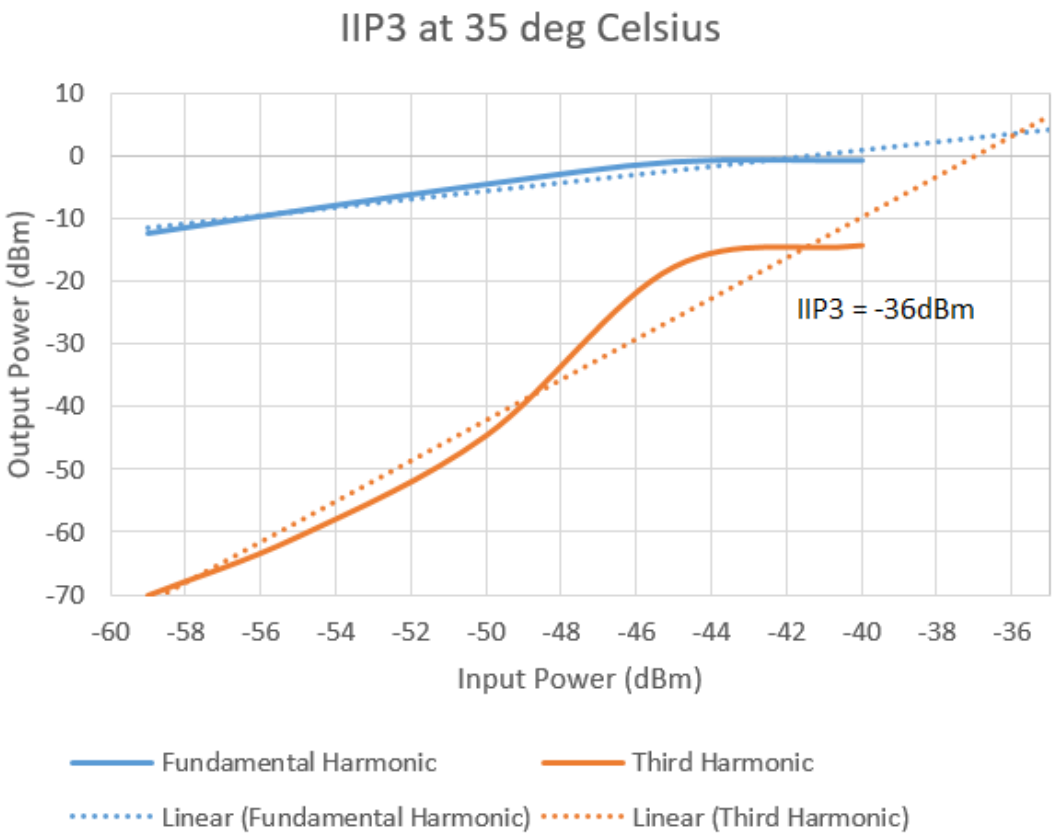

Figure 4.13 IIP3 plot for 35^0C temperature

4.4 Power Consumption

The current drawn by the board for a power supply of 3.5V for different temperatures has been shown in the table below. This current is majorly drawn by the amplifier. The power consumption due the current drawn by the digital control pins of the switches is negligible. We can see that temperature does not affect power consumption much.

Table 4.1 Power Consumption at different temperatures

Temperature (degree Celsius)	Current (milli Ampere)	Voltage (Volts)	Power (milli Watts)
15	151	3.5	528.5
25	153	3.5	535.5
35	154	3.5	539

CHAPTER 5

CONCLUSION AND FUTURE WORK

While designing a PCB for space we have to take into consideration many factors which affect the circuit differently in space as opposed to designing it for a ground-based project. One such considerations was the type of switch to be used for the design of the EDGES receiver. The current receiver uses a mechanical switch which has the advantage of low insertion loss. But this cannot be continued in the EDGES In Space project as these switches have a limited life time. We want a switch that lasts longer without degrading the performance. The solution to this would be electrical switches which have the advantage of faster switching time and ideally do not degrade in performance with time. But these switches have higher insertion loss. This is a major change that will have to be made moving forward. The board was designed using the electrical switches and we see that the Noise Figure, which is expected to be affected most by the electrical switches is in a tolerable range. We also get the added advantage of the small size of the switches, which is what we are aiming for in this design.

We also get a high gain by cascading two amplifiers. We consume 535mWatts of power to achieve this gain. The power consumption is slightly more than what would be suitable for a space project. But this can be easily achieved by replacing the amplifier with one that runs on lesser power. These amplifiers were not considered for this project due their poor input reflection coefficient. If we replace the amplifiers, we would have to have a more complicated input matching network. The input matching network could add to the noise figure, but if designed aptly a good input reflection coefficient can be obtained without degrading the Noise Figure by a lot.

This project implements only the low-band equivalent of the EDGES project. The switches and amplifiers used in this project have excellent performance in the EDGES high-band instrument frequency range as well. By just changing the filter and implementing a wide-band input matching network this project can be extended to the EDGES high-band equivalent.

With the placement followed in this design the calibration standards used to measure the reflection coefficient of the antenna are not placed equally away from the VNA. This can be easily corrected for by measuring the insertion loss at each path and correcting for each path separately. This is not of major concern for our frequency range of operation, but if the high-band instrument were to be implemented the correction may not remain the same at higher frequencies. This will add to the extra requirement of correcting for each calibration standard for different frequencies. If we ensure that the trace length between the VNA and each calibration standard is same, this entire task of correcting for different losses can be avoided while implementing the high-band instrument in the same design

One main concern about the performance of this design in space would be how it would perform at varying temperatures. It gets very hot during the day due to the radiations from the sun and gets as cold as cryogenic temperatures at night. This board has only been tested for temperatures that the EDGES project operates in. Though the performance of this design does not vary a lot in these temperatures it many not perform the same in a much larger variation of temperatures. However, if the temperature control mechanism which is currently being implemented in the EDGES project is continued then good performance can be expected. The filter seems to be the most sensitive to temperature. It can be replaced by a filter built from lumped components less sensitive to temperature. This would also provide more real estate on the board as

currently the filter is the largest component on the board. This extra space can then be utilized to implement the temperature control mechanism or a more complex input matching network.

REFERENCES

[1] "Chronology of the universe," Wikipedia, The Free Encyclopedia, [Online]. Available: https://en.wikipedia.org/w/index.php?title=Chronology_of_the_universe&oldid=883437648. [Accessed 27 February 2019].

[2] "Timeline of the Universe," Planck Mission Cardiff university, [Online]. Available: http://planck.cf.ac.uk/science/timeline/universe/bigbang. [Accessed 27 February 2019].

[3] "Timeline of the Universe," Planck Mission Cardiff University, [Online]. Available: http://planck.cf.ac.uk/science/timeline/universe/inflation. [Accessed 27 February 2019].

[4] "Timeline of the Universe," Planck Mission Cardiff Univesity, [Online]. Available: http://planck.cf.ac.uk/science/timeline/universe/3minutes. [Accessed 27 February 2019].

[5] "Timeline of the Universe," Planck Mission Cardiff University, [Online]. Available: http://planck.cf.ac.uk/science/timeline/universe/cmb. [Accessed 27 February 2019].

[6] "Timeline of the Universe," Planck Mission Cardiff University, [Online]. Available: http://planck.cf.ac.uk/science/timeline/universe/dark-ages. [Accessed 27 February 2019].

[7] "Timeline of the Universe," Planck Mission Cardiff University, [Online]. Available: http://planck.cf.ac.uk/science/timeline/universe/first-stars. [Accessed 27 February 2019].

[8] "Timeline of the Universe," Planck Mission Cardiff University, [Online]. Available: http://planck.cf.ac.uk/science/timeline/universe/overview. [Accessed 27 February 2019].

[9] "Timeline of the Universe Image," National Aeronautics and Space Administration, [Online]. Available: https://map.gsfc.nasa.gov/media/060915/index.html. [Accessed 27 February 2019].

[10] "EDGES Science," Low Frequency Cosmology Lab, Arizona State University, [Online]. Available: http://loco.lab.asu.edu/edges/edges-science/. [Accessed 18 April 2019].

[11] U. P. P., H. R., D. K. and S. M., "Electron Spin," LibreTexts, [Online]. Available: https://phys.libretexts.org/Bookshelves/University_Physics/Book%3A_University_Physics_(OpenStax)/Map%3A_University_Physics_III_-_Optics_and_Modern_Physics_(OpenStax)/8%3A_Atomic_Structure/8.3%3A_Electron_Spin. [Accessed 18 April 2019].

[12] "Redshift," Wikipedia The Free Encyclopedia, [Online]. Available: https://en.wikipedia.org/wiki/Redshift. [Accessed 18 April 2019].

[13] "Epoch of Reionization," Murchison Widefield Array, [Online]. Available: http://www.mwatelescope.org/science/epoch-of-reionization-eor. [Accessed 27 February 2019].

[14] S. Zaroubi, "Epoch of Reionization," in *The First Galaxies*, Berlin, Heidelberg, Springer, 2013, pp. 45-101.

[15] D. DeBoer, A. Parsons, J. Aguirre, P. Alexander, Z. Ali, A. Beardsley, G. Bernardi, J. Bowman, R. Bradley, C. Carilli and C. Cheng, "Hydrogen Epoch of Reionization Array (HERA)," *Publications of the Astronomical Society of the Pacific*, vol. 129, no. 974, 2017.

[16] "EDGES - LoCo Lab," Low Frequency Cosmology Lab - Arizona State University, [Online]. Available: http://loco.lab.asu.edu/edges/. [Accessed 6 March 2019].

[17] J. Bowman and A. E. E. Rogers, "VHF-band RFI in Geographically Remote Areas," in *Proceedings of the RFI Mitigation Workshop*, Groningen, Netherlands, 2010.

[18] T. Mozdzen, J. Bowman, R. Monsalve and A. Rogers, "Improved measurement of the spectral index of the diffuse radio background between 90 and 190 MHz," *Monthly Notices of the Royal Astronomical Society,* 2016.

[19] R. A. Monsalve, A. E. E. Rogers, J. D. Bowman and T. J. Mozdzen, "Calibration of the EDGES High-band Receiver to Observe the Global 21 cm Signature from the Epoch of Reionization," *The Astrophysical Journal,* vol. 835, no. 1, 2017.

[20] A. E. E. Rogers and J. D. Bowman, "Absolute calibration of a wideband antenna and spectrometer for accurate sky noise temperature measurements," *Radio Science,* vol. 47, no. 4, 2012.

[21] T. Mozden, "http://loco.lab.asu.edu/memos/," 23 May 2018. [Online]. Available: http://loco.lab.asu.edu/loco-memos/edges_reports/tom_20180523_Calibration_Steps.pdf. [Accessed 07 March 2019].

[22] R. Monsalve, A. Rogers, J. Bowman and T. Mozdzen, "RESULTS FROM EDGES HIGH-BAND: I. CONSTRAINTS ON PHENOMENOLOGICAL MODELS FOR THE GLOBAL 21 CM SIGNAL," *The Astrophysical Journal,* vol. 847, no. 1, p. 64, 2017.

[23] J. Bowman, A. Rogers, R. Monsalve, T. Mozdzen and N. Mahesh, "An absorption profile centred at 78 megahertz in the sky-averaged spectrum," *Nature,* vol. 555, no. 7694, p. 67, 2018.

[24] T. C. Voytek, A. Natarajan, J. M. Jáuregui García, J. B. Peterson and O. López-Cruz, "Probing the Dark Ages at z ~ 20: The SCI-HI 21 cm All-sky Spectrum Experiment," *The Astrophysical Journal Letters,* vol. 782, no. 1, 2014.

[25] L. Philip, Z. Abdurashidova, H. C. Chiang, N. Ghazi, A. Gumba, H. M. Heilgendorff, J. Hickish, J. M. Jáuregui-García, K. Malepe, C. D. Nunhokee, J. Peterson, J. L. Sievers, V. Simes and R. Spann, "Probing Radio Intensity at high-Z from Marion: 2017 Instrument," *Journal of Astronomical Instrumentation,* 2018.

[26] S. Singh, R. Subrahmanyan, N. U. Shankar, M. S. Rao, B. S. Girish, A. Raghunathan, R. Somashekar and K. S. Srivani, "SARAS 2: a spectral radiometer

for probing cosmic dawn and the epoch of reionization through detection of the global 21-cm signal," *Experimental Astronomy*, vol. 45, no. 2, pp. 269-314, 2018.

[27] D. C. Price, L. J. Greenhill, A. Fialkov, G. Bernardi, H. Garsden, B. R. Barsdell, J. Kocz, M. M. Anderson, S. A. Bourke, J. Craig, M. R. Dexter, J. Dowell, M. W. Eastwood, T. Eftekhari, S. W. Ellingson, G. Hallinan, J. M. Hartman and Kimber, "Design and characterization of the Large-aperture Experiment to Detect the Dark Age (LEDA) radiometer systems," *Monthly Notices of the Royal Astronomical Society*, vol. 478, no. 3, pp. 4193-4213, 2018.

[28] M. Sokolowski, S. E. Tremblay, R. B. Wayth, S. J. Tingay, N. Clarke, P. Roberts, M. Waterson, R. D. Ekers, P. Hall, M. Lewis, M. Mossammaparast, S. Padhi, F. Schlagenhaufer, A. Sutinjo and Ti, "BIGHORNS - Broadband Instrument for Global HydrOgen ReioNisation Signal," *Publications of the Astronomical Society of Australia*, vol. 32, 2015.

[29] "Ionosphere," Wikipedia, The Free Encyclopedia, [Online]. Available: https://en.wikipedia.org/wiki/Ionosphere. [Accessed 05 March 2019].

[30] A. Datta, R. Bradley, J. O. Burns, G. Harker, A. Komjathy and T. J. W. Lazio, "Effects Of The Ionosphere On Ground-Based Detection Of The Global 21 CM Signal From The Cosmic Dawn And The Dark Ages," *The Astrophysical Journal*, 2014.

[31] M. &. B. A.-J. Bentum, "Low frequency astronomy — The challenge in a crowded RFI environment," in *XXXth URSI General Assembly and Scientific Symposium*, 2011.

[32] J. O. Burns, J. Lazio, J. Bowman, R. Bradley, C. Carilli, S. Furlanetto, G. Harker, A. Loeb and J. Pritchard, "Probing the first stars and black holes in the early Universe," *Advances in Space Research*, vol. 49, no. 3, pp. 433-450, 2012.

[33] J. Silk, "Put Telescopes on the far side of the Moon," nature International Journal of Science, 03 January 2018. [Online]. Available: https://www.nature.com/articles/d41586-017-08941-8. [Accessed 05 March 2019].

[34] J. O. Burns, J. Lazio, J. Bowman, R. Bradley, C. Carilli, S. Furlanetto, G. Harker, A. Loeb and J. Pritchard, "Probing the First Stars and Black Holes with the Dark Ages Radio Explorer (DARE)," *American Astronomical Society*, vol. 43, 2011.

[35] "Chang'e 4 - Satellite Missions," eoPortal Directory, [Online]. Available: https://directory.eoportal.org/web/eoportal/satellite-missions/c-missions/chang-e-4. [Accessed 05 March 2019].

[36] A. Boonstra, M. Wise, J. van der Marel, M. A. M. Ruiter, D. Prinsloo, J. Bast, G. Kruithof, H. Falcke, M. Klein-Wolt and C. Brinkerink, "The Netherlands - China Low Frequency Explorer," in *32nd International Union of Radio Science (URSI) General Assembly Scientific Symposium (GASS)*, Montreal, Canada, 2017.

[37] "Mini-Circuits MSP2TA-18-12+," [Online]. Available: https://www.minicircuits.com/pdfs/MSP2TA-18-12+.pdf. [Accessed 19 March 2019].

[38] "Analog Devices ADGM1304 Datasheet," [Online]. Available: https://www.analog.com/media/en/technical-documentation/data-sheets/adgm1304.pdf. [Accessed 19 March 2019].

[39] A. E. E. Rogers, "MIT Haystack Observatory: EDGES Memo Series," 30 January 2017. [Online]. Available: https://www.haystack.mit.edu/ast/arrays/Edges/EDGES_memos/116.pdf. [Accessed 20 March 2019].

[40] J. D. Bowman, A. E. E. Rogers, R. A. Monsalve, T. J. Mozdzen and N. Mahesh, "An absorption profile centred at 78 megahertz in the sky-averaged spectrum," *Nature*, vol. 555, pp. 67-70, 2018.

[41] "Mini-Circuits," [Online]. Available: https://www.minicircuits.com/pdfs/PHA-13LN+.pdf. [Accessed 20 March 2019].

[42] "MMBZ5221BLT1 - Zener Voltage Regulators," [Online]. Available: https://www.onsemi.com/pub/Collateral/MMBZ5221BLT1-D.PDF. [Accessed 26 March 2019].

[43] "PC/104 Specification - PC/104 Consortium," 13 October 2008. [Online]. Available: https://pc104.org/wp-content/uploads/2015/02/PC104_Spec_v2_6.pdf. [Accessed 26 March 2019].

[44] J. Coonrad, "Sending Circuit Materials Into Space," Microwave Journal, 2014.

[45] J. Coonrad, "Comparing Microstrip and Grounded Coplanar Waveguide," Microwave Journal, 2015.